ARTICLES
https://doi.org/10.1038/s41551-020-0538-5

nature biomedical engineering

Check for updates

A retrievable implant for the long-term encapsulation and survival of therapeutic xenogeneic cells

Suman Bose[1], Lisa R. Volpatti[1,2,9], Devina Thiono[1,3,9], Volkan Yesilyurt[1,3], Collin McGladrigan[1,3], Yaoyu Tang[1,3], Amanda Facklam[1], Amy Wang[2], Siddharth Jhunjhunwala[1,7], Omid Veiseh[1,8], Jennifer Hollister-Lock[4], Chandrabali Bhattacharya[1], Gordon C. Weir[4], Dale L. Greiner[5], Robert Langer[1,2,3,6] and Daniel G. Anderson[1,2,3,6] ✉

The long-term function of transplanted therapeutic cells typically requires systemic immune suppression. Here, we show that a retrievable implant comprising a silicone reservoir and a porous polymeric membrane protects human cells encapsulated in it after implant transplantation in the intraperitoneal space of immunocompetent mice. Membranes with pores 1 μm in diameter allowed host macrophages to migrate into the device without the loss of transplanted cells, whereas membranes with pore sizes <0.8 μm prevented their infiltration by immune cells. A synthetic polymer coating prevented fibrosis and was necessary for the long-term function of the device. For >130 days, the device supported human cells engineered to secrete erythropoietin in immunocompetent mice, as well as transgenic human cells carrying an inducible gene circuit for the on-demand secretion of erythropoietin. Pancreatic islets from rats encapsulated in the device and implanted in diabetic mice restored normoglycaemia in the mice for over 75 days. The biocompatible device provides a retrievable solution for the transplantation of engineered cells in the absence of immunosuppression.

Cell-based therapy has the potential to revolutionize the treatment of chronic diseases such as autoimmune disorders, endocrine disorders, neurological degeneration and cancer[1–3]. Engineered cells can simultaneously detect pathological conditions and act as living factories to manufacture and deliver drugs that treat diseased tissue[2]. Cells can be programmed to deliver a variety of therapeutics in the form of small molecules, proteins[4], exosomes[5] and viruses[6]. Implanted cells containing synthetic gene circuits have alleviated allergic responses[7], cured diabetes[4] and treated Parkinson's disease[5] in rodent models. Recent advances in stem cell technology have made it possible to generate unrestricted quantities of functional pancreatic β cells[8,9], making islet replacement therapy a clinically viable option. However, a major roadblock for the translation of these cell-based therapies is the lack of a safe and effective technology for transplanting these cells within patients[3,10].

Therapeutic cells can be immunogenic to the host[2,3,11]. Cell encapsulation has been broadly investigated as a method to allow transplantation of cells without chronic immunosuppression[10]. Microencapsulation of cells in natural[10] or synthetic hydrogel beads[12] is one method for immune isolation. Despite the potential of microencapsulation, the development of a single macroencapsulation device may enable greater control of the three-dimensional structure and facilitate device retrieval. This may be particularly important when transformed cells are used with tumorigenic potential, including human embryonic stem cell-derived cells, which can contain undifferentiated cells that may form teratomas[10].

One approach to developing a retrievable encapsulation device has been to reinforce alginate gel with polymeric fibres[13,14]. These millimetre-scale devices offer the advantage of high permeability to nutrients and have already shown promising results in pre-clinical models. However, the lack of rigidity may cause difficulty in maintaining the device shape[10], in addition to the risk of graft escaping from the alginate gel. Macrodevices made out of durable polymeric materials can overcome these limitations and offer greater flexibility with the shape and configuration of the implant, but have been challenging to develop.

In a typical immune-isolating macrodevice, the transplanted cells are protected by a membrane that blocks various elements of the immune system[10,15,16]. The membrane pore size is critical for proper macrodevice function as it should be designed to selectively block harmful immune components while offering minimum resistance to the transport of oxygen, nutrients and the secreted therapeutic factors[10]. An optimal cell encapsulation device will enable a rapid response to environmental cues, such as secreting insulin in response to blood glucose change[15,16]. Effectors of the immune system span over four orders of magnitude in size (cytokines: ~2 nm; cells: ~10 μm) and there continues to be debate around which elements of the immune system need to be blocked from access to the cells[16,17]. While it is clear that direct contact with immune cells

[1]David H Koch Institute for Integrative Cancer Research, Massachusetts Institute of Technology, Cambridge, MA, USA. [2]Department of Chemical Engineering, Massachusetts Institute of Technology, Cambridge, MA, USA. [3]Department of Anesthesiology, Boston Children's Hospital, Boston, MA, USA. [4]Section on Islet Cell and Regenerative Biology, Research Division, Joslin Diabetes Center, Boston, MA, USA. [5]Program in Molecular Medicine, University of Massachusetts Medical School, Worcester, MA, USA. [6]Institute of Medical Engineering and Science, Massachusetts Institute of Technology, Cambridge, MA, USA. [7]Present address: Centre for BioSystems Science and Engineering, Indian Institute of Science, Bengaluru, India. [8]Present address: Department of Bioengineering, Rice University, Houston, TX, USA. [9]These authors contributed equally: Lisa R. Volpatti, Devina Thiono. ✉e-mail: dgander@mit.edu

must be prevented, there is a lack of evidence on the requirement for blocking cytokines[15]. Previous studies developed size-exclusion membranes with pores <20 nm in diameter that can block cytokines and antibodies. Despite promising results in vitro, these cytokine-blocking membranes did not prevent graft loss in vivo[18,19].

Polymeric membranes with pores up to 400 nm in diameter have been investigated in the construction of encapsulation devices because of their ability to prevent infiltration of immune cells[10,20,21]. Interestingly, studies on cell migration have reported that cells are unable to squeeze through confined spaces <7 μm² in cross-sectional area (~3-μm-diameter circular pores) without matrix degradation[22]. We reasoned that micrometre-sized pores might provide cell barrier function while allowing for high permeability. However, the upper limit on the membrane pore size that can maintain immune barrier function was unclear.

Another challenge to macrodevice function in vivo is the potential of a foreign body reaction to result in fibrosis and cellular isolation[19–21]. Materials commonly used for fabricating macrodevices induce a foreign body reaction to the implant[16]. Additionally, it is generally held that immunogenic antigens shed by the encapsulated cells can intensify the fibrotic response, making xenotransplants more difficult than allotransplants[15,16]. The foreign body reaction is a complex process that involves activation and recruitment of several types of cells, such as macrophages and fibroblasts, to the implant site, eventually leading to deposition of a collagenous fibrotic capsule around the device[23]. The fibrotic capsule limits the supply of oxygen and nutrients to the encapsulated cells and induces cell death due to hypoxia. Recently chemical structures have been identified that substantially limit fibrosis in rodents and non-human primates[24]. These improved materials have enabled the long-term function of microencapsulation devices with islets in both rodents and non-human primates[25,26].

Fibrosis-induced hypoxia remains a major barrier for macrodevices and various strategies have been explored to overcome this[10]. The TheraCyte device used a composite membrane comprising an inner immune-isolating membrane and an outer membrane with larger pores designed to induce neovascularization[20]. While early tests in rats were encouraging, a recent phase I clinical trial with a modified version of this device (marketed as VC-01 by ViaCyte) revealed extensive fibrosis and cell death in 17 of the 19 patients receiving an implant[27]. Promising strategies for improving vascularization have been explored for hydrogel-based devices[28,29], but they remain to be tested on macrodevices in fibrotic animal models. Other approaches have involved perfusing the implanted macrodevice with external oxygen to maintain normoxia within the device chambers[30], and repeated filling of the implanted macrodevice with therapeutic cells through an external catheter[31]. While these strategies are promising, the requirements for cell maintenance and contact with the external environment limit their clinical potential. Therefore, there is a need for the development of macrodevices that do not fibrose.

Here, we develop a biocompatible macrodevice that can serve as a technology to deliver and maintain immunogenic therapeutic cells in vivo over long periods. In our modular device, we sequentially improve membrane characteristics and biocompatibility to enable device performance. We establish a pore size cut-off for membranes to maintain their cell barrier function. We also develop a surface modification technique to graft anti-fibrotic molecules on our devices and demonstrate a surface coating that can mitigate the fibrotic response over long periods. Finally, we demonstrate the efficacy of the device with human cell lines and rat islets in immunocompetent mouse models.

Results

Device development and in vitro characterization. The device comprises a cell reservoir attached to a thin porous polymeric membrane (Fig. 1a). Details of device fabrication are included in the Methods. A flexible silicone elastomer (polydimethylsiloxane (PDMS)) is used to cast the device, which contains a microfabricated cell reservoir along with microchannels for injection of cells into the device. Finally, a polycarbonate track-etched (PCTE) membrane is chemically bonded to the device[32]. The assembled device is loaded with cells through an access port and sealed using an ultraviolet curable adhesive. The microfabricated reservoir has a depth of 150 μm (similar to the distance between capillaries[33]) and allows precise positioning of the cells close to the membrane, ensuring optimal diffusion of nutrients. The reservoir contains PDMS pillars, which prevent collapse of the membrane onto the PDMS surface, and aid in uniform filling of the microchamber with cells during the device loading process (see Supplementary Fig. 1 for a three-dimensional model of the device). PCTE membranes are mechanically robust and can be manufactured with pores of distinct sizes and narrow size distribution[34]. The device is flexible, allowing safe implantation within soft tissues such as the peritoneum without the risk of injury.

The device supports the growth of several cell lines in vitro, including human embryonic kidney HEK293 cells, 3T3 fibroblasts and C2C12 myoblasts (Fig. 1b,c). Scanning electron microscopy (SEM) images of the device cross-section showed encapsulated cells tightly packed inside the cell reservoir (Fig. 1b). Confocal imaging of the encapsulated cells though the PDMS body (see Supplementary Fig. 1 for experimental setup) showed three-dimensional structures formed by the cells within the device, confirming survival of the cells (Fig. 1c). Since implanted human cells can invoke a xenogeneic response in rodents[35], we sought to examine the utility of our device with human cells in immunocompetent mice. HEK293T cells were transformed to constitutively secrete mouse erythropoietin (HEKepo cells) (Supplementary Fig. 2). Erythropoietin (EPO)—a hormone that drives red blood cell production in the bone marrow—is used to treat anaemia in chronic kidney disease and chemotherapy[36]. Moreover, EPO is also a useful hormone evaluating the activity of therapeutic cells. A short plasma half-life (<6 h in rodents) and high bioavailability[37] of EPO results in a good correlation between the EPO concentration in the serum and the number of viable therapeutic cells secreting EPO.

HEKepo cells encapsulated in the device were cultured for 4 weeks, while the secretion rate of EPO from the device was measured periodically. Increasing EPO secretion was seen in the first 2 weeks, which plateaued afterward (Fig. 1d) to a steady-state rate of 0.4–0.6 μg of EPO per day, which we expected to achieve a therapeutic effect[38]. We found that although the secretion rate of EPO from cells was not affected by encapsulation (Supplementary Fig. 2), the proliferation rate of cells rapidly dropped inside the device over the first week, possibly due to metabolic restriction on cell growth due to limited available space and nutrients (Supplementary Fig. 3). The encapsulated cells remained confined within the device when membranes with a pore size of ≤1 μm was used, but readily escaped from pores with a diameter of 3 μm (Supplementary Fig. 4).

Determining membrane pore size for immune protection. Membrane pore size is a critical parameter governing immune isolation, and ultimately device function. Pores with large diameters favour increased diffusion of macromolecules and other large payloads (exosomes and viruses) across the membrane, but risk compromising the immune barrier function of the membrane. Despite several suggestions[10,39], the upper limit of the membrane pore size that can maintain immune barrier function and prevent the destruction of encapsulated cells by the host immune system remained to be determined.

To do this, we used BALB/c mice, which are immune competent and have been extensively used to study acute allo- and xenograft rejection[40]. Devices were fabricated using PCTE membranes with nominal pore sizes of 3, 1, 0.8, 0.6 and 0.4 μm. The membrane

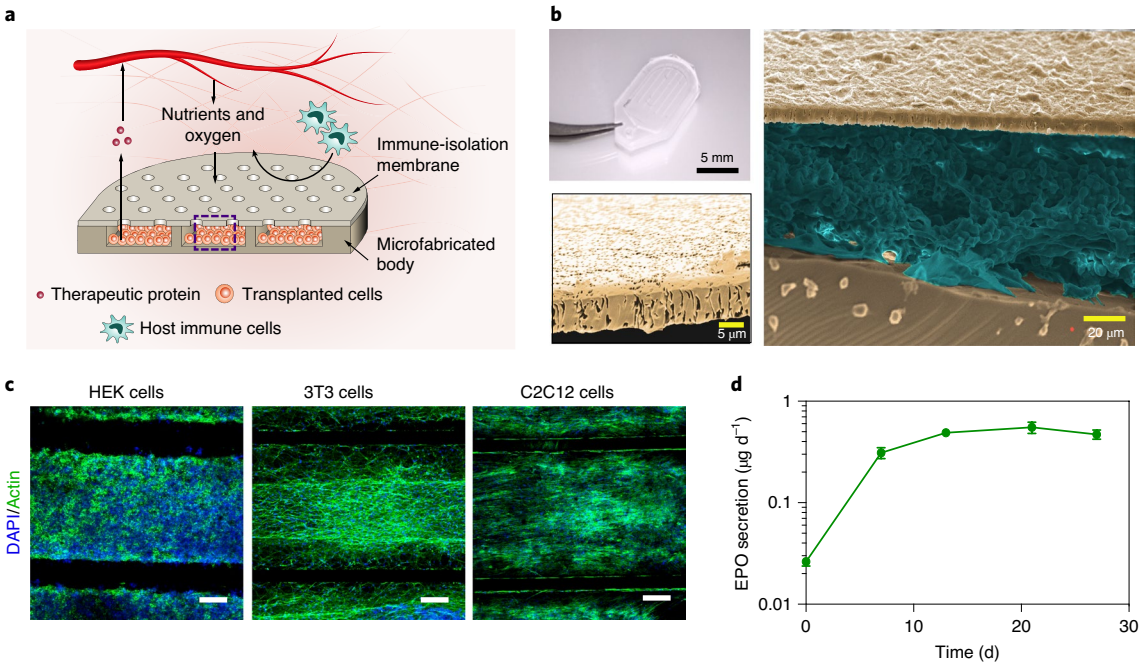

Fig. 1 | Overview of an implantable macrodevice and its pre-clinical development. a, Schematic of the device design and operation. The device consists of a microfabricated body sealed to a polymeric membrane with a controlled pore size, which allows the exchange of macromolecules but prevents infiltration of immune cells. **b**, Pre-clinical realization of the macrodevice. Top left: view of the device used in the pre-clinical testing in mice. Right: false-coloured SEM image of the device cross-section, showing the polymeric membrane, reservoir-containing cells and the silicone body of the device. Bottom left: false-coloured SEM image of the membrane cross-section. **c**, Z-stack confocal images showing human embryonic kidney (HEK293T) cells, mouse fibroblasts (3T3 cells) and myoblasts (C2C12 cells) within the sealed devices cultured in vitro for 7 d. Scale bars, 200 μm. **d**, Rate of EPO production over time by devices encapsulating HEKepo cells and cultured in vitro. In total, 0.25 million HEKepo cells were encapsulated per device ($n = 7$ devices) and the EPO concentration was measured in culture supernatants over a period of 12 h for each time point. Data points and error bars represent means ± s.e.m.

permeability was equal among the groups by varying the pore density, to rule out differences in oxygen transport. Devices loaded with HEKepo cells were transplanted into the intraperitoneal space of BALB/c mice, and EPO concentrations in the serum were monitored weekly. We found that the serum EPO level more than doubled in all animals by 2 d post-transplantation and continued to increase through the first week (Fig. 2a). The devices were functional in vivo, allowing survival and growth of the encapsulated cells, and successfully delivered EPO. After the first week, devices with a pore size of 3 μm failed, as EPO levels eventually returned to baseline, while other groups remained functional with a steady increase in serum EPO levels.

We suspected that the 3-μm pores allowed infiltration of immune cells, as reported previously[41], causing graft rejection. To verify our hypothesis, we retrieved the implanted devices after 5 weeks and immunostained them to identify macrophages (F4/80 cells) and T cells (CD3 cells). We used confocal microscopy to image the encapsulated cell reservoir within intact devices. The HEKepo cells expressed red fluorescent protein (RFP), which was used to identify grafted cells. As expected, we found extensive infiltration of macrophages and T cells, along with complete loss of the graft, inside the 3-μm devices (Fig. 2b,c). In contrast, devices with a pore size of ≤0.8 μm had no infiltration of immune cells, and large aggregates of HEKepo cells were seen (Fig. 2b,c and Supplementary Fig. 2).

Interestingly, membranes with a pore size of 1 μm prevented entry of T cells but allowed infiltration of macrophages inside the device. The HEKepo cells were found intact despite direct contact with the infiltrated macrophages. This was a startling observation and we wanted to ascertain the size of the pores that allowed macrophage infiltration into the device. The rated pore sizes of PCTE membranes are determined by the bubble point method, which might underestimate the pore cross-section area—a parameter relevant for cell migration. Therefore, SEM imaging was used to analyse the membranes and determine the pore cross-sectional area. We found that all of the membranes had a wide distribution in the pore cross-sectional area, with considerable overlap between membranes of different groups (see Supplementary Discussion and Supplementary Fig. 6). Based on the distribution, it seemed likely that pores with an area between 1.00 and 1.25 μm^2, which are unique to the 1-μm membrane (that is, not present on the 800 nm membranes), are responsible for selective infiltration of macrophages. Cells have only been known to migrate through confined spaces with a minimum cross-section of 7 μm^2 (diameter: ~3 μm)[22] or higher[42], and this report of cells migrating though pores 1.25 μm^2 in area is below that limit in vivo.

Lastly, we tested for an antibody response against the graft, and found that by 5 weeks all of the groups had high levels of circulating HEKepo-specific immunoglobulin G (IgG) antibodies (Fig. 2d,e). Since our membranes are not permselective for antibodies (pores are 100-fold greater in size than antibodies[39]), our results indicate that a humoral response alone was not sufficient to cause notable graft damage. Also, a membrane pore size cut-off of 0.8 μm (pore area < 1 μm^2) was determined to be adequate for preventing immune cell infiltration and graft failure in our model. However, commercial membranes can potentially contain larger defects affecting long-term experiments. Therefore, we decided to use 0.4-μm rated membranes in our further studies.

Developing a biocompatible surface coating. Biocompatibility of the implanted device is an important feature that affects in vivo function. Foreign body response (FBR) to the implanted device has the potential to damage the graft in two ways: direct cytokine assault

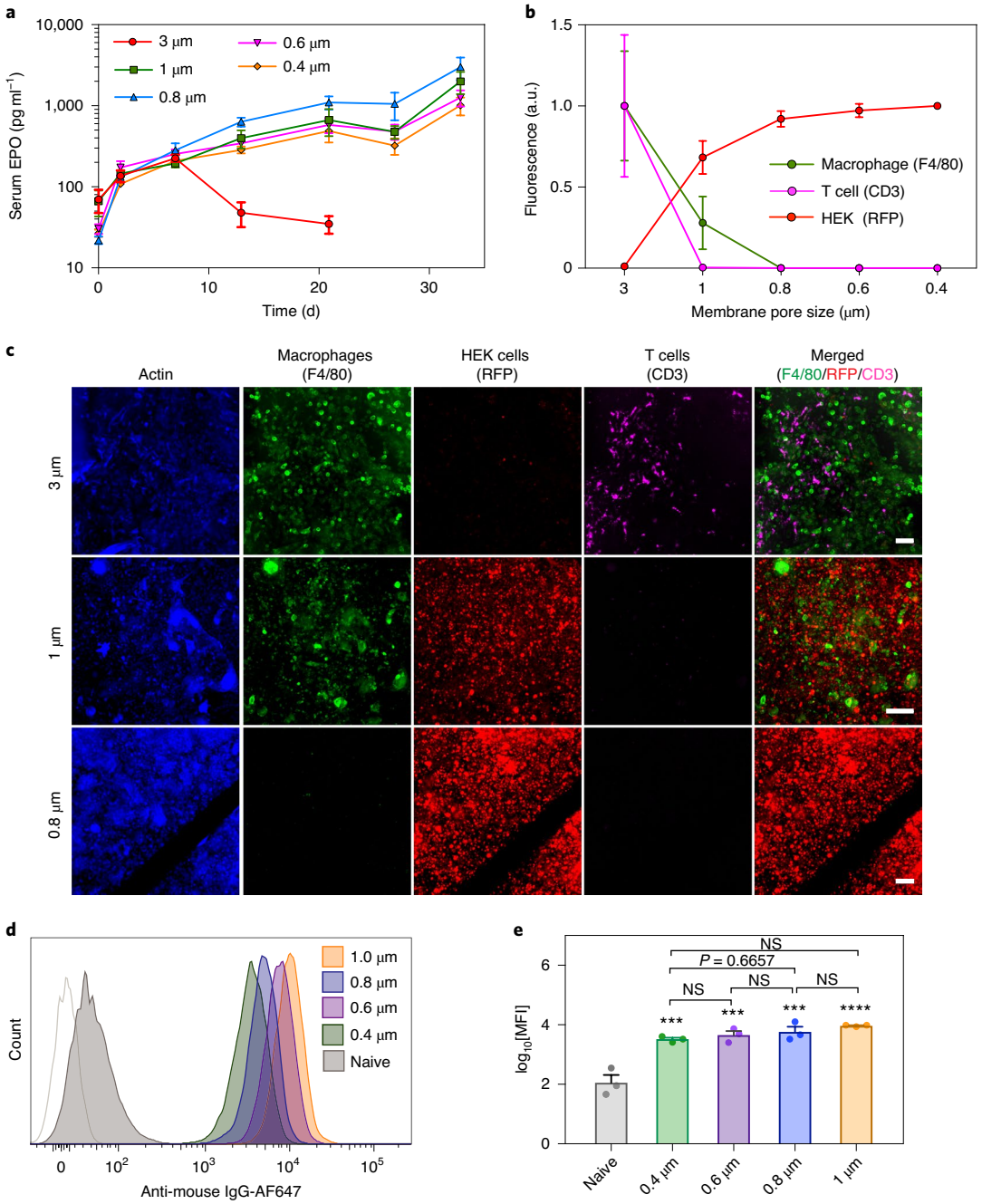

Fig. 2 | Membrane pore size regulates immune cell infiltration and survival of xenografts in BALB/c mice. a, Time course of the serum concentration of EPO in BALB/c mice after intraperitoneal transplantation of HEKepo cells encapsulated within macrodevices with different membrane pore sizes ($n = 4$ animals per group). Devices with 3-μm pores fail rapidly, whereas pore sizes of ≤1 μm protect the grafted cells. Data points and error bars represent means ± s.e.m. **b**,**c**, The retrieved devices (after 35 d) were immunostained for actin (cytoskeleton; blue), macrophages (F4/80; green), HEKepo cells (RFP; red) and T cells (CD3; magenta), after which confocal microscopy was used to image and identify the cells present inside the reservoir volume of the devices ($n = 3$ animals per group). Total fluorescence (normalized) quantification (**b**) and representative Z-stack images (**c**) show complete infiltration of immune cells through the 3-μm membranes, leading to widespread loss of graft, while 1-μm membranes selectively allowed infiltration of macrophages but not T cells, preventing graft damage. All pore sizes of ≤800 nm prevented immune cell infiltration (Supplementary Fig. 5). Scale bars, 100 μm. These experiments were repeated twice with similar results. **d**,**e**, Detection of graft-specific antibody in the serum. HEKepo cells incubated with animal serum (day 35) were counterstained with anti-mouse IgG-AF647 and analysed using flow cytometry (**d**), which showed the presence of cell-specific antibodies in the serum of all of the animals receiving the devices. Quantification of the mean fluorescence intensity (MFI; **e**) showed significant levels of anti-graft IgG in animals with the devices compared with untreated (naive) animals ($n = 3$ animals per group). The experiments were repeated twice. Bar heights and error bars represent means ± s.e.m. Statistical significance was determined by one-way ANOVA with Bonferroni multiple comparison correction (***$P < 0.001$ and ****$P < 0.0001$ in comparison with the naive group; NS, not significant ($P > 0.999$)).

and through deposition of a fibrotic capsule causing hypoxia[10]. Materials commonly used in the construction of macrodevices are poorly biocompatible and previous studies have noted significant fibrosis on implanted devices[43], impacting their success. To address this issue, we set out to develop a surface coating that can enhance device biocompatibility and mitigate the FBR. Zwitterionic polymers

demonstrate anti-fouling properties and coatings of zwitterionic polymers on biomaterials have reduced FBR in rodents and large animal models[44–46]. Zwitterionic head groups can significantly affect biocompatibility[46], so we decided to test three major classes of zwitterionic polymer coatings: poly(phosphorylcholine) (developed from methacryloyloxylethyl phosphorylcholine (MPC)), poly(carboxybetaine) (developed from carboxybetaine methacrylate (CBMA)) and poly(sulfobetaine) (developed from sulfobetaine methacrylate (SBMA)) (Fig. 3a). In another recent study, a combinatorial screen identified a small-molecule modification of alginate, which showed notable improvement in the biocompatibility of alginate hydrogels in rodents and non-human primates[24]. We postulated that the small molecule tetrahydropyran phenyl triazole (THPT) might act as an anti-fibrotic coating, and decided to test it on our devices along with the zwitterionic polymers. Devices were coated through surface-initiated atom transfer radical polymerization (ATRP), which allowed controlled growth of dense polymer brushes from the surface (Fig. 3a). X-ray photoelectron spectroscopy (XPS) analysis confirmed a high degree of polymer grafting on the surface of the device (Supplementary Fig. 7 and Supplementary Table 1)[47]. Modification of the surface properties was confirmed with contact angle measurements, which showed significant reduction in water contact angle values. The zwitterionic coatings made the devices significantly hydrophilic with contact angle values of ~10°. SEM imaging of the device further confirmed the presence of the polymer coating on the device surface (Supplementary Fig. 8). The coating did not appear to affect the permeability of the membranes significantly (Supplementary Fig. 9).

Next, we directly tested the efficacy of each coating for improving device performance in C57BL/6 mice—a fibrotic a mouse model[48]. Coated and uncoated devices loaded with HEKepo cells were implanted in the intraperitoneal space of C57BL/6 mice, with empty devices serving as a control. We found that by 4 weeks the THPT-coated group had achieved the highest serum EPO levels (195.7 pg ml^{-1}), which were significantly greater than the levels for the uncoated (69.84 pg ml^{-1}) or empty device (72.3 pg ml^{-1}) (Fig. 3b). In contrast, the MPC coating was the most effective among the three zwitterionic coatings, but only modestly increased serum EPO levels. Thus, we selected THPT as the biocompatible surface coating on our devices. Since surface coatings can degrade under harsh conditions, we wanted to test the long-term stability of the THPT coating in the in vivo environment. Surface analysis of implanted materials is challenging due to the deposition of proteins and cells, which can mask the actual chemical composition of the surface. To overcome this challenge, we used confocal Raman spectroscopy to analyse the surfaces of devices retained in vivo for 4 weeks. The characteristic peak for the triazole ring[49] was used to confirm the presence of the THPT coating, as this moiety is absent in physiological molecules. We found no significant change of characteristic peaks after retrieval of the device (Supplementary Fig. 11), confirming that the THPT coating is retained for at least 4 weeks in vivo.

Effect of the surface coatings on FBR. We investigated how the THPT coating might improve the survival of encapsulated cells. Visual examination of the explanted devices (after 4 weeks in vivo) revealed moderate to heavy fibrosis and extensive tissue overgrowth on uncoated and zwitterionic-coated devices, while the THPT-coated devices remained clean with only a thin collagenous capsule (Fig. 3c,d). Masson's trichrome staining of device cross-sections showed a 150- to 250-μm-thick fibrotic capsule on the uncoated membranes, while this was only 30–50 μm on the THPT-coated membranes (Fig. 3c). The zwitterionic-coated membranes had varying degrees of fibrosis, with MPC being the best of the zwitterionic coatings. Quantification of the collagen deposition on the devices correlated with the histological findings and confirmed that the THPT coating had the best anti-fibrotic efficacy, resulting in a 70% reduction in collagen buildup (Fig. 3c).

To understand how the surface coatings might alter the immune response to the device, we performed gene expression analysis using a NanoString assay on the RNA extracted from explanted devices, and measured the relative abundance of genes associated with FBR. We found that each coating had a unique pattern of gene expression compared with uncoated devices (Fig. 3e). Notably, the THPT coating suppressed the expression of the pro-inflammatory cytokines tumour necrosis factor-α and interleukin-1β (which are typically associated with classically activated macrophages) and CD146 (a marker for neovascularization). Proteomic analysis of proteins extracted from the device surface using the iTRAQ (isobaric tag for relative and absolute quantitation) method detected 11 isoforms of collagen, three isoforms of fibrinogen, fibronectin, laminin and other extracellular matrix proteins, all of which were substantially reduced on the THPT-coated devices (Fig. 3f). Finally, we immunostained the devices for myofibroblasts (α-smooth muscle actin (α-SMA)), T cells (CD3), macrophages (F4/80) and F-actin (cytoskeleton) and used confocal microscopy to analyse the cellular deposit on the device membranes. We found that the THPT-coated membranes had markedly reduced cellular overgrowth compared with untreated membranes (Fig. 4a). Direct measurement of total DNA content on the device surface was significantly lower on THPT-coated devices, further supporting the microscopy results (Fig. 4b). Together, these results suggest that the THPT coating possibly alters the immune response, resulting in reduced secretion of pro-inflammatory cytokines and lower cellular recruitment to the device, finally leading to a mitigated fibrotic response.

Fig. 3 | A biocompatible surface coating minimized foreign body reaction and prevents device failure in C57BL/6 mice. a, Schematic of the chemistry scheme used to modify device surface with biocompatible polymers. Surface-initiated activators regenerated by electron transfer (ARGET) ATRP was used to grow polymer brushes of four different monomers (CBMA, SBMA, MPC and THPT), the structures of which are shown to the right. **b**, Serum concentration of EPO in C57BL/6 mice 28 d after intraperitoneal transplantation with surface-modified (coated) devices encapsulating HEKepo cells (1×10^6 per device). Uncoated devices with or without cells (empty) were used for comparison. The THPT-coated devices showed the highest increase in serum EPO compared with the other coatings. Bar heights and error bars represent means ± s.e.m, Group sizes (animals) were: $n=7$ (SBMA), $n=9$ (MPC) and $n=10$ (empty, uncoated and THPT). The results represent combined data from two independent experiments. Statistical significance was determined by one-way ANOVA with Bonferroni multiple comparison correction. *P* values are shown for comparison with empty devices. **c**, Collagen deposition on retrieved devices, quantified by hydroxyproline assay of proteins extracted from the device surface, showing the lowest hydroxyproline deposition on THPT-coated devices. Bar heights and error bars represent means ± s.e.m. ($n=5$ animals). Statistical significance was determined by one-way ANOVA with Bonferroni multiple comparison correction. *P* values are shown for comparison with the THPT group. **d**, Representative images of the retrieved devices. Bright-field images of intact devices are shown at the top, along with histological sections of the device membranes (bottom; Masson's trichrome staining). Minimal fibrosis was found on the THPT-coated devices. Scale bars: 5 mm (top), 100 μm (bottom). The experiments were repeated twice with similar results. **e**, NanoString-based analysis of the expression of phenotypic markers in cells attached to the device surface 28 d post-transplantation. Values are normalized to uncoated devices and presented on a $\log_2$ scale ($n=5$ animals per group). IFN-γ, interferon-γ; MCAM, melanoma cell adhesion molecule. **f**, Relative proteomic analysis of the protein lysates extracted from retrieved devices, showing levels of major proteins of the extracellular matrix. Values are expressed as the fold change compared with uncoated devices.

Demonstration of the long-term sustained release of therapeutic proteins in vivo. THPT-coated and uncoated devices were loaded with 2×10^6 HEKepo cells and transplanted in the intraperitoneal space of C57BL/6 mice. The control group received THPT-coated devices without cells. We found that the serum EPO levels in the THPT group increased steadily over the first 10 weeks, reaching ~500 pg ml^{-1} (an increase of about eightfold), and remained high for the duration of the study (130 d) (Fig. 5a). The results show that THPT-coated devices can successfully maintain the viability and function of xenografts for over 4 months. The biphasic trend in serum EPO levels recapitulated our in vitro observations (Fig. 1d) and may be attributed to the restricted growth of cells due to overcrowding inside the device and cellular aging. The THPT coating did not prevent a humoral response, as high levels of circulating antibodies against the HEKepo cells were detected in the sera of all animals (Supplementary Fig. 12) similar to earlier observations (Fig. 2d). In contrast, the uncoated device failed to increase serum EPO in the first 10 weeks, probably due to FBR to the device, which resulted in damage to the grafted cells (Fig. 5a). However, a modest rise in serum EPO was observed in the later part of the study, which

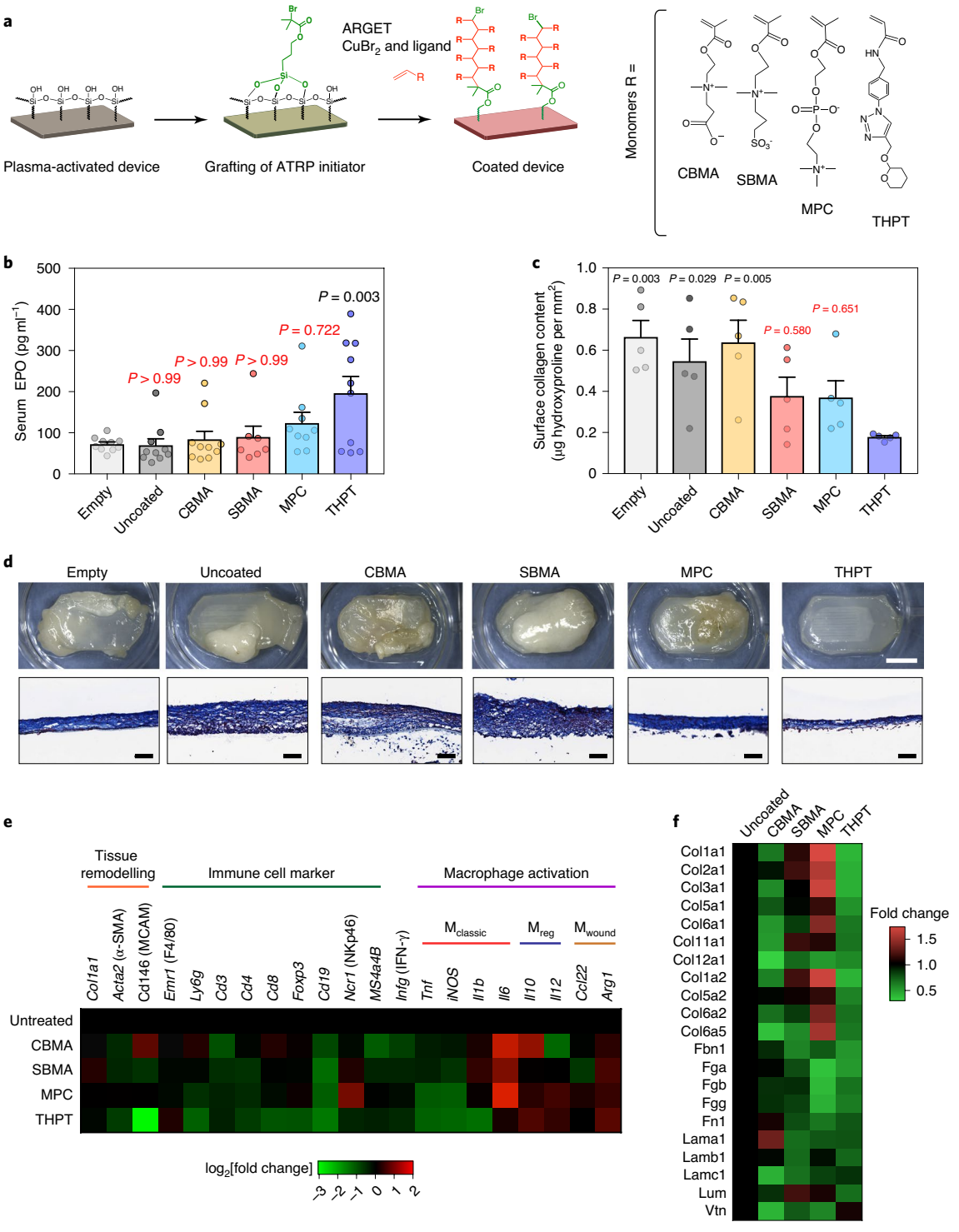

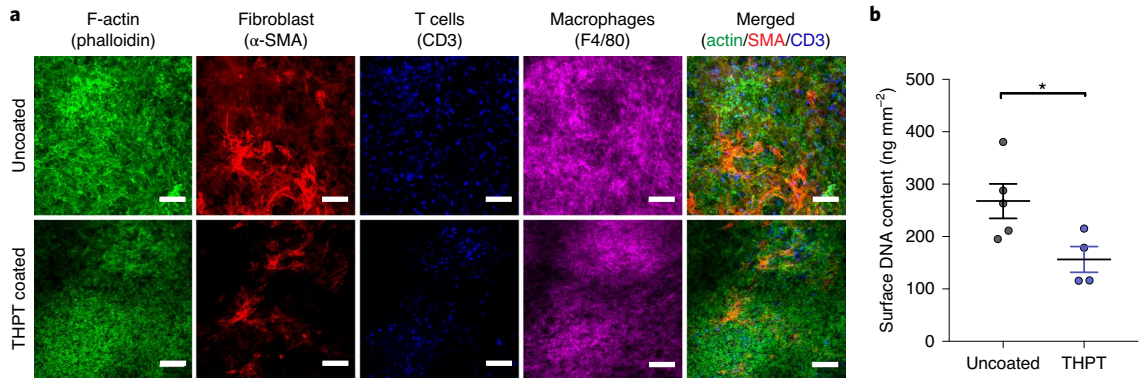

Fig. 4 | THPT coating reduces cellular buildup on the implanted devices. a, Representative immunofluorescent Z-stack confocal images showing cytoskeleton (actin; green), fibroblast (α-SMA; red), T cells (CD3; blue) and macrophages (F4/80; magenta) within the fibrotic layer on the membranes of the uncoated and THPT-coated devices shown in Fig. 3. Significantly lower amounts of staining can be seen on the THPT membranes. Scale bars, 100 µm. These experiments were repeated three times. **b**, Quantification of the total DNA extracted from the cells attached to the surfaces of the THPT-coated and uncoated devices. Amounts of extracted DNA were normalized to the device surface area. Sample sizes were: $n=5$ animals (uncoated) and $n=4$ animals (THPT). Data points and error bars represent means ± s.e.m. Statistical significance was determined by unpaired, two-tailed *t*-test (*$P=0.024$).

might indicate recovery of the surviving cells from the initial damage and their subsequent proliferation within the device.

An increase in blood haematocrit levels is another indicator of therapeutic delivery of EPO[50] and can reflect long-term serum EPO levels. Measurements of haematocrit showed a steady rise in haematocrit values, indicating a robust performance by the THPT-coated devices. Haematocrit values in the THPT group were significantly higher than in the uncoated device group (Fig. 5b). To better evaluate the efficacy of our device in maintaining high red blood cell production and treating anaemia, we set a therapeutic goal of maintaining the haematocrit at supraphysiological levels (>70%), which can only be achieved through the sustained delivery of EPO[50]. The THPT group showed a significantly better response to treatment compared with the uncoated group, with >95% of animals achieving the therapeutic goal by the end of the study (Fig. 5c). Examination of the retrieved devices at the end of the study (130 d) revealed that the uncoated devices were heavily fibrosed while the THPT-coated devices remained relatively clean (Fig. 5d), indicating that the THPT coating can provide durable protection against fibrosis.

Demonstration of device retrieval. Macrodevices simplify the removal of the implant to allow rapid withdrawal of therapy[10]. To demonstrate this, we implanted devices loaded with HEKepo cells in the intraperitoneal space of C57BL/6 mice through a laparotomy procedure. After retaining them for 10 weeks, we performed another laparotomy procedure to extract the devices. The THPT-coated devices could be easily located and retrieved without apparent distress to the animals. In contrast, extensive adhesion to internal organs was noted on many of the uncoated devices, preventing their safe removal.

Removal of the THPT-coated devices resulted in a sharp drop in serum EPO, which returned to pre-surgery levels within 1 week (Fig. 5e). To confirm that the explanted devices contained viable cells, we measured the EPO secretion rates of the devices in vitro after retrieval and compared them with the secretion rate measured before implantation. We found that the secretion rate of the THPT devices increased over the 10-week period in vivo, indicating survival and proliferation of the encapsulated cells. An opposite trend was seen with the uncoated devices, for which the secretion rate declined over the same period (Supplementary Fig. 13). These data provide direct evidence that the THPT coating is essential for the survival of the encapsulated graft.

Long-term regulated delivery of therapeutic proteins using tetracycline-inducible engineered cells. For some diseases, it is desirable to have therapeutics on demand in order to more precisely follow a dosing regimen. Cells engineered to produce therapeutics that are regulated by doxycycline offer one way to achieve this. Oral delivery of doxycycline (an antibiotic) can rapidly turn on the secretion of proteins in transplanted engineered cells harbouring the inducible gene[51]. To demonstrate this proof of concept, we first developed HEK cells with doxycycline-inducible EPO secretion (see Methods). In vitro characterization showed excellent control over EPO secretion, with minimal secretion in the absence of doxycycline and a 50-fold increase in secretion upon exposure to physiologically relevant doxycycline concentrations (Supplementary Fig. 14). The doxycycline-inducible HEKepo cells were loaded inside THPT-coated devices and transplanted intraperitoneally in C57BL/6 mice, where they were retained for 130 d. To determine the ability of the device to deliver EPO on demand, animals were switched from a regular diet to a doxycycline-containing diet (200 mg kg^{-1}) for 3 d every alternate week. The EPO concentration was measured weekly. We found that while serum EPO remained at normal levels with a regular diet, it increased by more than five-fold with a doxycycline diet (Fig. 5f). The serum EPO remained responsive to doxycycline induction throughout the study (130 d), indicating that the encapsulated cells maintained their activity. Importantly, we could maintain haematocrit levels at physiological levels throughput the experiment with controlled delivery of EPO (Supplementary Fig. 15).

Macroencapsulation of islets. Islets isolated from Sprague–Dawley rats were loaded inside THPT-coated or uncoated devices (200–300 islet equivalents per device). Since naked islets do not survive well without a supporting matrix[52], we loaded the islets in an alginate solution, which was later crosslinked in situ by dipping the device in a barium bath (see Methods). The devices were transplanted intraperitoneally in streptozotocin (STZ)-induced diabetic C57BL/6 mice, and blood glucose measurement was used to monitor islet function over time non-invasively. While both groups achieved euglycaemia (blood glucose ≤ 200 mg dl^{-1}) immediately post-transplantation, the majority of uncoated devices failed within 3 weeks (median: 19.5 d), resulting in hyperglycaemia (Fig. 6a and Supplementary Fig. 16). In contrast, the median graft survival time, as determined by maintenance of normoglycaemia of the THPT-coated group, was 75 d post-transplantation. The blood glucose levels and fraction cured of the animals receiving THPT devices were significantly better compared with those of the animals receiving uncoated devices (Fig. 6a,d).

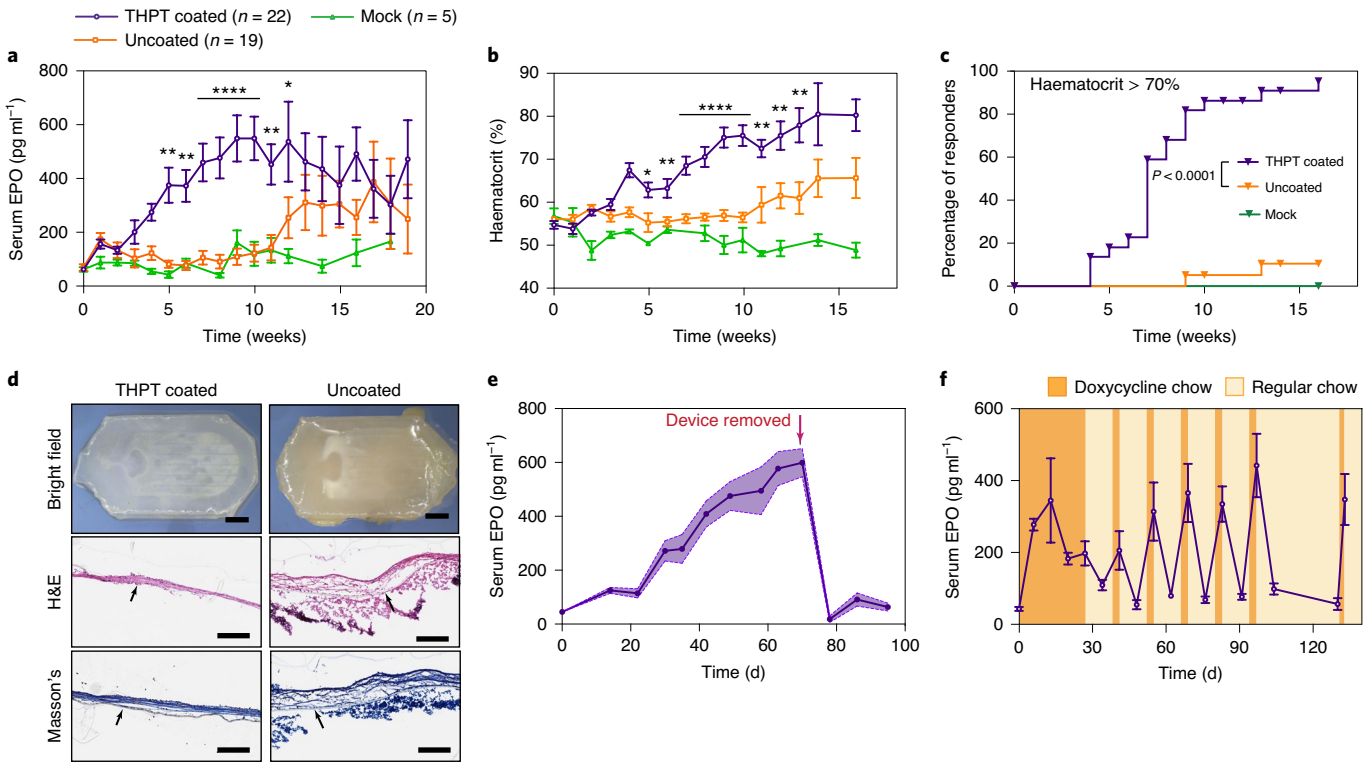

Fig. 5 | Long-term delivery of EPO in C57BL/6 mice in a sustained or on-demand manner, using coated macrodevices encapsulating HEKepo cells. **a**–**c**, Efficacy of THPT-coated devices in the long-term sustained delivery of EPO. Serum concentrations of EPO (**a**) and haematocrit (**b**) were measured over time in C57BL/6 mice after intraperitoneal transplantation of THPT-coated or uncoated macrodevices encapsulating 2×10^6 HEKepo cells. Empty THPT-coated devices were used as mock transplants. THPT-coated devices showed excellent efficacy in elevating serum EPO and haematocrit, while the uncoated devices showed only limited success. Data points and error bars represent means ± s.e.m. Statistical significance for the comparison between THPT-coated and uncoated devices at each time point was determined by unpaired, two-tailed *t*-test (*$P < 0.05$; **$P < 0.01$; ****$P < 0.0001$). The Kaplan–Meier plot in **c** shows the fraction of animals with haematocrit ≥ 70% over the course of treatment. There was a significantly better response with the THPT-coated devices. Group sizes (animals) were $n = 22$ (THPT), $n = 19$ (uncoated) and $n = 5$ (mock). The results represent combined data from three independent experiments. Significance was determined by two-sided log-rank (Mantel–Cox) test ($P < 0.0001$). **d**, Representative bright-field and histology images of the devices in **a**, retrieved after 130 d. The THPT-coated devices remained biocompatible, with only a thin fibrotic capsule. Histological sections showed fibrosis on the device membrane with haematoxylin and eosin (H&E) staining (middle) and Masson's trichrome staining (bottom). The membrane is indicated by a black arrow. Scale bars: 2 mm (top) and 200 μm (middle and bottom). **e**, Time course of the serum EPO concentration after C57BL/6 mice were implanted with THPT-coated devices encapsulating HEKepo cells. Animals maintained high EPO levels until devices were explanted (day 70; indicated by an arrow), after which the EPO levels promptly returned to baseline levels. The data points represent group means ($n = 5$ animals), while the shaded region represents the s.e.m. **f**, On-demand delivery of EPO was achieved by encapsulating doxycycline-inducible HEKepo cells within THPT-coated devices and transplanting them in the intraperitoneal space of C57BL/6 mice. A doxycycline diet (orange shaded regions) resulted in a sharp rise in serum EPO concentrations. This was rapidly reversed by switching to a normal diet (yellow regions). The data points and error bars represent means ± s.e.m ($n = 5$ animals).

To evaluate the kinetics of insulin release from the device, we performed an intravenous glucose tolerance test on the animals for the first 3 weeks post-transplantation (Fig. 6b,c and Supplementary Fig. 17). Although both devices functioned similarly in the first week, differences between the THPT-coated and uncoated devices started to emerge from the second week onwards (Fig. 6b and Supplementary Fig. 17b). The THPT devices demonstrated an excellent glycaemic profile similar to that of healthy animals (Fig. 6b,c), while the uncoated devices had a poor glycaemic profile and did not achieve euglycaemia over the 120 min of the study. A rise in serum insulin levels in response to glucose challenge was also significant in the THPT group (Supplementary Fig. 17). In a subset of animals, we explanted THPT-coated devices 35 d post-transplantation. All of the animals exhibited a prompt return of diabetes immediately following device removal, confirming that the cure was device dependent (Supplementary Fig. 18). Imaging of the explanted devices showed viable islet clusters within the device, along with a few scattered dead cells, indicating the successful immune protection offered by the THPT-coated device. Although the reason for the failure of the device during the late phase of the study is unclear, device fibrosis did not appear to be the cause since the THPT-coated devices retrieved at the end of the study were found to have minimal fibrotic deposition (Supplementary Fig. 19). It is more likely that the number of islets used was insufficient for a long-term cure[53] and they could not accommodate an increase in the body weight (~20–40%) of the animals over the study period[54].

Discussion

We have developed a modular biocompatible macrodevice that can maintain xenografts in immunocompetent animals over long periods. To demonstrate the broad potential of this microfabricated device, we first showed that it is able to protect engineered human cells secreting EPO in C57BL/6 mice for at least 130 d (Fig. 5a–c). Using transgenic human cells with an inducible gene circuit, the device was also adapted to provide on-demand therapeutic protein in response to orally dosed small molecules (Fig. 5f). Approaches

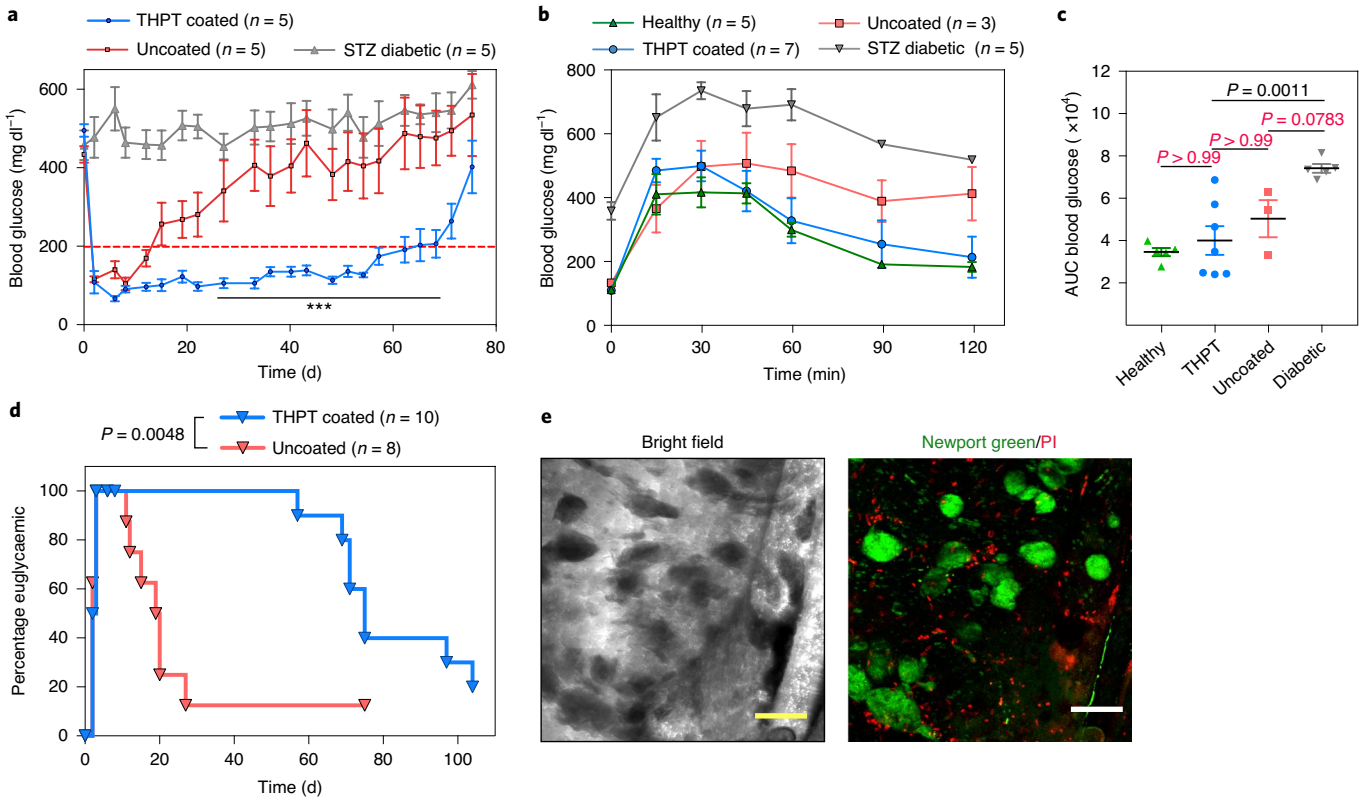

Fig. 6 | Efficacy of the coated macrodevice encapsulating rat islets in curing STZ-induced diabetic C57BL/6 mice. a, Blood glucose curves showing prolonged euglycaemia with the THPT-coated devices. In contrast, success was short lived with the uncoated devices, resulting in significantly higher blood glucose levels. The devices encapsulated 200–300 islet equivalents, with $n = 5$ animals in each group. The experiments were repeated twice. Data points and error bars represent means ± s.e.m. Statistical comparison between the THPT-coated and uncoated devices at each time point was determined by unpaired, two-tailed *t*-test (***$P < 0.001$). The red dashed line indicates the blood glucose cutoff for normoglycaemia in mice (200 mg dl^{-1}). **b**,**c**, An intravenous glucose tolerance test was performed on healthy and diabetic mice 15 d post-transplantation. There was no significant delay in blood glucose correction for the THPT group and healthy mice, while the uncoated devices failed to correct blood glucose during the 120 min (**b**). Area-under-the-curve (AUC) analysis (**c**) showed significant improvement with the THPT-coated devices in blood glucose kinetics. The data points (**b**) and horizontal bars (**c**) represent means, whereas error bars represent s.e.m. Statistical significance in **c** was determined by one-way ANOVA with Bonferroni multiple comparison correction. **d**, Kaplan–Meier plot showing the fraction of euglycaemic (blood glucose < 200 mg dl^{-1}) STZ-C57BL/6 mice after receiving rat islets within THPT-coated or uncoated devices. Statistical significance was determined by two-sided log-rank (Mantel–Cox) test ($P = 0.0048$). **e**, Live/dead staining with Newport Green (stains insulin granules) and propidium iodide (PI) (dead cells), confirming the viability of encapsulated islets inside THPT-coated devices retrieved from STZ-C57BL/6 mice 35 d post-transplantation. The experiments were repeated twice with similar results. Scale bars, 200 µm.

like this may enable the simple implementation of therapies when irregular dosing of protein therapeutics is required. Finally, we show that encapsulated rat islets were capable of restoring euglycaemia for more than 75 d in diabetic mice (Fig. 6a,d). While additional engineering may be needed to enable longer-term survival of islets, this study provides proof of the principle that cell therapies secreting therapeutics in response to endogenous environmental cues can also be incorporated into this device.

To optimize the transport properties, we identified an upper limit on the membrane pore size for maintaining immune isolation properties. Commercial PCTE membranes with a rated pore diameter ≤0.8 µm could prevent infiltration of immune cells and offer long-term protection to encapsulated human cells in vivo. Since the cells were encapsulated without any supporting matrix, the polycarbonate membrane seems sufficient for immune protection. We discovered that infiltration of immune cells could be selectively regulated by tuning the membrane pore size, with pores possibly between 1 and 1.25 µm^2 in area allowing selective macrophage infiltration but blocking T cells. Recent research has highlighted the crucial role of macrophages in graft repair and protection[55]. Macrophages are also important for β cell regeneration in vivo and may actually be beneficial for islet transplantation[56]. Therefore, the ability to selectively recruit beneficial macrophages to the graft without rejection may provide new methods of affecting cell-based therapies.

A key component of device design was the need to reduce the fibrotic response (Fig. 3b). The zwitterionic coatings (despite their potent anti-fouling properties[44]) did not improve the biocompatibility of our devices. While the failure mode is unclear, we note that the presence of xeno-antigens can aggravate the immune reaction, and may have provided a confounding factor. The THPT coating described here provided durable protection against fibrosis and was required to enable the long-term survival of cells (Fig. 5a). While the original chemistry was identified in a screen of modified alginate polymers, we found it surprising that the addition of a small fragment of this modification would enable resistance to fibrosis on a completely different material. Since fibrosis is a common challenge with other micro- and macro- cell encapsulation devices[10,15,16], we believe the ability to use this coating on different devices may facilitate the function of other cell delivery systems. The THPT coating might allow membranes with larger pore sizes to retain immune isolation properties, and this needs further investigation.

We further hypothesize that this approach may be applicable to a wide variety of medical devices, such as catheters, breast implants, sensors and drug delivery devices.

Methods

Material and reagents. All chemicals were obtained from Sigma–Aldrich and the cell culture reagents were obtained from Life Technologies, unless otherwise noted. The silicone elastomer Sylgard 184 was obtained from Dow Corning (catalogue number 3097358-1004). Polycarbonate (PCTE) membrane filters (hydrophobic; polyvinylpyrrolidone-free) with a diameter of 25 mm were obtained from Sterlitech. The silane initiator for ATRP was (3-trimethoxysilyl)propyl 2-bromo-2-methylpropionate (catalogue number SIT8397.0; Gelest). HEK292T cells were purchased from the American Type Culture Collection. Pre-packaged lentivirus for cell transfection was purchased from AMS Biotechnology (mouse EPO LVP496; tetracycline-inducible construct LVP017-Hygro). Pre-coated EPO ELISA plates were purchased from BioLegend (catalogue number 442780). The antibodies used (Alexa Fluor 687-conjugated anti-mouse F4/80 (clone BM8), BV421-conjugated anti-mouse CD3 (clone 17A2) and Alexa Fluor 647-conjugated anti-mouse IgG (catalogue number 405322)) were purchased from BioLegend. Cy3-conjugated anti-mouse α-SMA antibody (clone 14A) was purchased from Sigma–Aldrich. F-actin-specific Alexa Fluor 488-conjugated Phalloidin, DAPI, propidium iodide, SYTOX Blue, Newport Green and the Click-iT EdU Alexa Fluor 647 cell proliferation kit (C10424) were purchased from Life Technologies. The Cell Titer Glo Luminescent Cell Viability Assay was purchased from Promega. THPT-acrylate monomer was custom synthesized from pharmacon and obtained with >98% purity, as determined by mass spectrometry and NMR. CBMA (3-[[2-methacryloyloxy)ethyl] dimethylammonio] propionate) and MPC (2-(methacryloyloxy)ethyl 2-(trimethylammonio)ethyl phosphate) monomers were purchased from TCI America. NOA81 ultraviolet curable glue was obtained from Norland Products.

Transformation and maintenance of cell lines. HEK293T, 3T3 and C2C12 cells were purchased from the American Type Culture Collection and cultured in Dulbecco's modified Eagle's medium (high glucose) supplemented with 10% foetal bovine serum (FBS) and 1% penicillin-streptomycin at 37 °C with 5% CO_2.

HEKepo cells. HEK293T cells were transformed with lentivirus expressing mouse EPO under a modified cytomegalovirus promoter also carrying an RFP- blasticidin fusion selection gene. Cells were transfected at a multiplicity of infection of 50:1 in media containing polybrene (5 μg ml^{-1}) for 24 h, after which cells were selected against blasticidin (20 μg ml^{-1}) for 3 weeks. Finally, the population was sorted by fluorescence-activated cell sorting (FACS) to collect the top 10% of the RFP-expressing cells in order to select for the clones with the highest expression of EPO. The RFP expression and in vitro EPO secretion were found to be stable over time, even upon withdrawal of blasticidin. Therefore, we cultured the HEKepo cells in normal cell culture media.

Dox-inducible HEKepo cells. The modified cytomegalovirus promoter used in the EPO construct carries two copies of tetracycline-operator elements, which normally do not interfere with expression, but can repress the action of the promoter in the presence of tetracycline repressor protein (TetR). The HEKepo cells selected earlier were transfected with lentivirus for constitutive expression of TetR protein according to the manufacturer's protocol, and selected in hygromycin media (800 μg ml^{-1}) for 3 weeks. The cell line was characterized in vitro for sensitivity to doxycycline and stability of protein production.

Rat islets isolation. Male Sprague–Dawley rats from Taconic, weighing approximately 300 g, were used for harvesting islets. All rats were anaesthetized with an injection of 1:20 xylazine (10 mg kg^{-1}) to ketamine (150 mg kg^{-1}) given intraperitoneally. The bile duct was cannulated and the pancreas was distended by an in vivo injection of 0.15% liberase in RPMI 1640 media solution. Rats were sacrificed by cutting the descending aorta and the distended pancreatic organs were removed and held in 50 ml conical tubes on ice until the completion of all surgeries. All tubes were placed in a bath of 37 °C water for a 30-min digestion. This was stopped by adding 10–15 ml of cold RPMI 1640 media (with 10% heat-inactivated FBS) and lightly shaking. Digested pancreases were washed twice in RPMI media, filtered through a 450-μm sieve and then suspended in a Histopaque-1077 and centrifuged at 1,700 RCF at 4 °C. Finally, the islets were collected from the gradient and further purified by gravity sedimentation. Purified islets were hand counted by aliquot under a light microscope and then washed three times in sterile 1× phosphate-buffered saline (PBS). Islets were then cultured in RPMI 1640 media with 10% heat-inactivated FBS and 1% penicillin-streptomycin overnight for further use.

Fabrication of devices. The device was designed using AutoCAD software and the photomask was printed on Mylar films at 50,000 dots per inch by a third-party vendor (Fineline Imaging). Photolithography was then used to make the master mould of the device. A 150-μm-thick film of SU8-2050 (Microchem) was spin-coated on a silicon wafer, ultraviolet exposed in a Karl Suss MA4 photoaligner and developed using PM Acetate. The height of the structure was determined by a Dektak surface profilometer and was found to be within 10% of the target height. Then, wafers were rendered inert by treating with Trichloro(1H,1H,2H,2H-perfluorooctyl)silane in a vacuum chamber for 6 h. PDMS prepolymer was mixed at a 10:1 ratio with the crosslinking agent, degassed and poured on the silicon wafer at a fixed volume such that the thickness of the PDMS layer was between 0.8 and 1 mm. The PDMS layer was cured at 60 °C overnight, peeled from the wafer and cut to shape to produce the PDMS chips. Inlet holes were made using a 0.75-mm biopsy punch (Harris Uni-Core; Ted Pella), following which the PDMS chips were cleaned using ethanol and dried.

PCTE membranes (25 mm in diameter) were cut in half and silanized by heating in 5% (v/v) solution of (3-aminopropyl)trimethoxysilane in water at 90 °C for 1 h. Silanized membranes were washed in deionized water and then ethanol to remove excess silane. The membranes were dipped in 1% HCl solution for 30 min to generate surface silanol groups and then stored in deionized water. To bond the membranes, the PDMS chips were activated with air plasma (Harris Plasma chamber) for 70 s. Silanized membranes were briefly wetted with 70% ethanol and laid over the activated PDMS chips. The devices were carefully heated to 60 °C in a high-humidity chamber for 3 h followed by overnight baking at 120 °C for the silane crosslinking to complete and form a stronger bond between the PCTE membrane and the PDMS chips.

Surface modification of devices. A special reaction chamber was custom designed and devices were placed in a manner that ensured proper exposure of the device surfaces to the reactants. The reaction mixture was constantly agitated for proper mixing. Devices were first grafted with an ATRP initiator by treating with air plasma for 70 s and incubating in a silane bath with 95% ethanol, 3% water (pH 4.5) and 2% (3-trimethoxysilyl)propyl 2-bromo-2-methylpropionate overnight at room temperature. The devices were washed with ethanol and dried on a hot plate before proceeding to the ATRP reaction.

Activators regenerated by electron transfer ATRP. We optimized the concentration of monomer, ligand and Cu(II) for each reaction so as to enable maximum surface grafting. The reaction mixture was prepared by dissolving 5 μmol Cu(II) bromide (0.5 mM), 20 μmol ligand (2 mM) and 20 μmol free initiator (ethyl-α-bromoisobutyrate; 2 mM) in 10 ml anhydrous methanol. The final concentration of the zwitterionic monomers (CBMA and SBMA) was 500 mM, while it was 100 mM for the THPT monomer. After screening a number of commercially available ATRP ligands, we found that TPMA (tris(2-pyridylmethyl)amine) worked the best for the CBMA and SBMA coating reactions, while Me4Cyclam (1,4,8,11-tetramethyl-1,4,8,11-tetraazacyclotetradecane) was ideal for THPT coating. The ATRP mixture was deoxygenated by three freeze–thaw cycles and charged into a nitrogen-purged reaction chamber. The ATRP was initiated by injecting 0.3 mmol Sn(II) 2-ethylhexanoate though a syringe, and the reaction was stirred at room temperature for 6 h. The Sn(II) 2-ethylhexanoate acts as a mild reducing agent producing $Cu(I)^+$ ions, which catalyses the polymer growth in a controlled manner. After 6 h, the devices were removed from the solution and washed 2× in methanol, followed by a wash in sterile 10× PBS (to dissolve the deposited polymers), then deionized water (sterile) and finally 70% ethanol, after which they were air dried in a sterile environment.

ATRP of MPC. We found that, unlike other monomers, the best coating with the MPC monomer was obtained through a traditional ATRP approach. To modify the devices with MPC, monomer (2 g; 6.78 mmol) and 12 ml 1:1 mixture of methanol and distilled water were added to a 25-ml Schlenk flask. This reaction mixture was sealed with a rubber septum stopper and placed in an ice bath. After degassing the reaction solution with nitrogen for 20 min, the ice bath was removed and CuBr (9.7 mg; 0.067 mmol) and bpy (21.15 mg; 0.135 mmol) were added to the reaction mixture under a strong nitrogen flow. Then, the mixture was charged into a nitrogen-purged reaction chamber containing the devices and allowed to react for 3 h at room temperature under a continuous weak nitrogen flow. Finally, the devices were removed, washed and prepared as descried previously.

Loading of the devices. The devices were sterilized by immersion in 70% ethanol for 1 h and drying under a sterile environment at room temperature. The cells were loaded into pre-sterilized devices using aseptic techniques. The devices had a total fill volume of 15 μl.

HEKepo cells. For EPO delivery, each device was loaded with 2×10^6 HEKepo or HEKepo-TetR cells (unless otherwise mentioned). The cells were harvested from culture flasks using a standard cell culture procedure and resuspended at a final concentration of 2×10^8 cells ml^{-1} in cell culture media inside a 1.5-ml centrifuge tube. A Hamilton gastight glass syringe with a 27-G cemented needle (to reduce cell loss during injection) was used to inject 10 μl of the cell suspension into each device. Following this, 5 μl NOA81 ultraviolet glue (loaded into a plastic Norm-Ject 1-ml syringe with a 23-G blunt needle) was injected to form a plug at the inlet. The device was then exposed to 365 nm ultraviolet light (EA-180; Spectroline) for 10 s with the clear PDMS side facing the ultraviolet source. This exposure was sufficient to cure the glue without causing any cell damage. Sealed devices were immediately immersed in media and cultured in 12-well plates.

Rat islets. In our initial experiments, we found that rat islets required a supportive matrix for survival inside the device. Therefore, we decided to use alginate as

the cell loading matrix since it is clinically approved, non-degrading and has been extensively used in islet transplantation. Rat islets were harvested and encapsulated the same day to prevent loss. Islets were washed in Hanks' Balanced Salt Solution (HBSS; Ca/Mg free) two times to remove the media, and counted. The islets were then aliquoted into individual 1.5-ml microcentrifuge tubes, with each tube carrying ~2,500 islets. The islets were pelleted and the supernatant was carefully removed. Finally, the islets were resuspended in 100 µl of 2% solution of a sodium alginate PRONOVA SLG20 (NovaMatrix) dissolved in 0.9% sterile saline (pH 7.4) to yield a final concentration of ~25 islet equivalents per µl. About 15 µl of the islet–alginate suspension was then loaded into each macrodevice using a digital microdispenser (Drummond; catalogue number 3-000-525), which ensured minimal islet loss during the injection process. The loaded devices were immediately immersed in a Ba^{2+} solution (20 mM $BaCl_2$ in HBSS) for 20 min to crosslink the alginate inside the device. Since the barium diffuses through the membrane into the device and crosslinks the alginate, care was taken such that the membrane was wetted properly immediately after contact with the solution as any trapped bubbles would prevent the entry of barium. The devices were washed in fresh HBSS for 10 min, transferred to 12-well plates with media (RPMI 1640 and 10% FBS) and cultured overnight.

In vitro culture of cells inside macrodevices. Sealed macrodevices loaded with cells were cultured in a 12-well plate for short-term culture (1–5 d or overnight before implantation) with 2 ml media replaced every 2–3 d. For long-term culture (>1 week), the devices were cultured in 6-well plates with 5 ml media. Culture media was replaced every 2 d. During cell culture, care was taken to orient the device such that membrane side faced towards the media (or allowed the supply of nutrients) while the PDMS side sat on the bottom of the plate. In some cases, two to three devices were cultured together in a 35-mm cell culture petri-dish with 12 ml media replaced every 3–4 d.

Implantation surgery. All animal procedures were approved by the Massachusetts Institute of Technology (MIT) Committee on Animal Care and supervised by MIT Division of Comparative Medicine veterinary staff. Male C57BL/6 mice, STZ-induced diabetic C57BL/6 mice and BALB/cJ mice of 6–8 weeks in age were obtained from The Jackson Laboratory and used in the experiments. Animals were anaesthetized with 3% isoflurane in oxygen. To prepare for surgery, the mice had their abdomens shaved and sterilized using betadine and isopropanol and were administered 0.03 mg Buprenorphine SR-LAB (ZooPharm) and 1 ml 0.9% saline subcutaneously. A small incision was made along the midline of the abdomen and blunt dissection was used to expose the peritoneal lining. An incision was made along the linea alba, and the device was transplanted in the abdomen, away from the fat pad. During transplantation, care was taken to orient the device such that the membrane faced the intraperitoneal organs while the PDMS side faced the abdominal wall. The incision was closed using 5-0 taper-tipped polydioxanone (PDS II) absorbable sutures. Skin was closed over the incision using a wound clip and tissue glue.

EPO measurement and blood glucose monitoring. EPO-producing HEK293 cell-loaded devices were incubated overnight in cell media and washed three times with HBSS (Gibco by Life Technologies) before transplantation surgery in healthy C57BL/6 mice. On the day of surgery and every week thereafter, 100 µl blood was collected from the medial saphenous vein in haematocrit tubes (catalogue number HP8H-10; SafeCrit) and blood collection tubes (catalogue number 365967; BD Microtainer). Haematocrit was processed using a micro-haematocrit centrifuge (StatSpin CritSpin; Beckman Coulter) and digital haematocrit reader (HemoCue America). After serum separation, the EPO concentration was measured using a Mouse EPO ELISA kit (catalogue number 442708; BioLegend).

Healthy C57BL/6 mice were treated with STZ by the vendor (The Jackson Laboratory) to induce type I diabetes before shipment to MIT. The blood glucose levels of all mice were tested preoperatively, and only mice with post-fasted blood glucose levels >350 mg dl^{-1} were considered diabetic and underwent transplantation. Blood glucose levels were monitored daily (with no fasting) for 3 d post-surgery and twice per week the following weeks after a 2-h fasting period. A small drop of blood was collected from a tail prick and tested using the commercial glucometer AlphaTRAK 2 (Zoetis) unless otherwise specified. Mice with a fasted blood glucose level <200 mg dl^{-1} were considered normoglycaemic. Monitoring continued until all mice had returned to the hyperglycaemic state, at which point they were euthanized and the devices were retrieved.

Mice were fasted for 6 h before the in vivo glucose tolerance test, with free access to water. Individual animals were given a bolus dose of 30% sterile glucose solution (in saline) at 1.5 g kg^{-1} through a tail vein injection using a 30-G insulin syringe (BD). Blood glucose was measured at 0, 15, 30, 60, 90 and 120 min after the injection. To assay for insulin levels, ~50–70 µl blood was collected from the medial saphenous vein in blood collection tubes before glucose infusion and at an appropriate time afterwards.

Retrieval of devices, cells and tissues. For non-terminal surgeries, the same implantation surgical procedure was used to retrieve the devices. For terminal studies, mice were euthanized using carbon dioxide administration, followed by cervical dislocation, at the desired time point. Implanted devices were recovered following necropsy, with care being taken to collect all of the tissue and cells adhered to the device. In the majority of cases, the implanted devices were found away from the site of implantation. While no clear pattern of migration of the device was noted, a notable number of devices were found either near the stomach or near the perigonadal fat pad. Upon retrieval, devices were washed with HBSS. Devices were either fixed (for use in microscopy and histology), flash frozen (for RNA, DNA or protein analysis) or cultured in vitro to determine the EPO production rate.

Imaging of retrieved materials. *Light microscopy.* Retrieved devices were washed with HBSS and transferred into 35-mm Petri dishes for bright-field imaging using a Leica stereoscopic microscope. For immunofluorescence imaging, fixed devices were washed twice with PBS, and cells were permeabilized with 0.1% Tween-20. After an additional wash with PBS, the devices were incubated with the staining solution containing the appropriate antibody cocktail (typical concentrations: 5 µg ml^{-1} for F4/80, 3 µg ml^{-1} for CD3 and 3 µg ml^{-1} for α-SMA) in 1% bovine serum albumin solution for 12 h at 4 °C. After 12 h, the devices were washed with PBS, transferred to a 70% glycerol solution in a glass-bottomed dish and imaged using an LSM 700 point scanning confocal microscope (Carl Zeiss).

Electron microscopy. Devices were washed in PBS and fixed in 10% glutaraldehyde solution overnight. Devices were then sectioned from the middle using a sharp razor and handled carefully thereafter. The samples were slowly dehydrated through a series of alcohol changes (10, 30, 50, 75, 90, 100 and 100%). The samples were then dried in a Critical Point Dryer (Tousimis Autosamdri-815) and loaded on aluminium pellets using carbon tape. The samples were coated with a 2-nm gold layer using a sputter coating system (Hummer 6.2) and images were recorded on a Jeol 5600LV scanning electron microscope.

Histological processing for haematoxylin and eosin and Masson's trichrome staining. Retrieved devices were fixed for 20 min using 4% paraformaldehyde at room temperature and washed 2× in PBS. The devices were cut in half in the middle using a sharp razor and stored in 70% ethanol for histological processing. The blocks were processed for paraffin embedding where care was taken to orient the sample such that histological sections of the device cross-sections could be obtained to reveal the thickness of the fibrotic capsule. The paraffin blocks were sectioned and stained according to standard histological methods.

Quantification of RNA, DNA, collagen and proteins. Freshly retrieved devices were segmented into two symmetrical segments along the lateral axis and immediately flash frozen and stored under liquid nitrogen until further use. One segment was processed using a DNA/RNA/Protein extraction kit (Qiagen) to retrieve the total DNA, RNA and protein from the sample. Another segment was processed for quantification of hydroxyproline, as detailed below. The segments were imaged using a Leica stereoscopic microscope to measure the total surface area of each portion that was later used in normalization of the surface DNA or hydroxyproline content.

Hydroxyproline assay. Devices were immersed in a 1:1 mixture of water and 37% hydrochloric acid and hydrolysed at 120 °C for 2 h. The resulting solution was used to determine the collagen concentration of each device using a hydroxyproline collagen assay kit (catalogue number MAK008; Sigma–Aldrich) according to the manufacturer's instructions.

DNA quantification. The total DNA extracted from the surface was measured using a Qubit dsDNA Quantification assay (Life Technology; catalogue number Q32851).

NanoString assay. RNA sequences extracted from the devices with different surface coatings ($n = 4$ per group) were quantified and diluted to the appropriate concentration (100 ng $µl^{-1}$). Then, 500 ng of each sample was processed according to the protocol of the manufacturer (NanoString) for expression analysis via our customized multiplexed gene panel. RNA levels (absolute copy numbers) were obtained following nCounter (NanoString) quantification, and group samples were analysed using nSolver analysis software (NanoString). Individual gene expression values were normalized to housekeeping genes (*Hprt*, *Bact* and *Cltc*). Relative fold changes were calculated by normalizing with the mean expression value of the uncoated devices, then log transformed.

Proteomics. For this assay, five samples were randomly selected from each device group. Equivalent amounts of protein (corresponding to similar surface areas from each sample) were reduced (10 mM dithiothreitol; 56 °C for 45 min) and alkylated (50 mM iodoacetamide; room temperature in the dark for 1 h). Proteins were subsequently digested with trypsin (sequencing grade; Promega). Trypsin activity was quenched by adding formic acid to a final concentration of 5%. Peptides were desalted using C18 SpinTips (Protea) then lyophilized and stored at −80 °C. Peptides were labelled with TMTsixplex (Thermo Fisher Scientific), per the manufacturer's instructions. Peptides were then loaded on a precolumn and separated by reverse-phase high-performance liquid chromatography (Easy nLC

1000; Thermo Fisher Scientific) over a 140-min gradient before nanoelectrospray using a Q Exactive mass spectrometer (Thermo Fisher Scientific). Raw mass spectral data files (.raw) were searched using Proteome Discoverer (Thermo Fisher Scientific) and Mascot version 2.4.1 (Matrix Science). Tandem mass tag (TMT) quantification was obtained using Proteome Discoverer and isotopically corrected per the manufacturer's instructions.

FACS analysis. *Anti-HEK IgG assay.* FACS was used to detect and quantify the levels of circulating IgG against transplanted HEKepo cells. Healthy and treated animals were bled to collect ~100 µl of serum. Then, 100,000 HEK cells were incubated with 100 µl tenfold-diluted serum (90 µl PBS and 10 µl serum) for 2 h at 4 °C. The cells were washed 2× with cold PBS and incubated with 100 µl anti-mouse IgG-Alexa Fluor 647 (5 µg ml^{-1}) for 30 min at 4 C. Finally, the cells were washed and analysed on an LSRFortessa flow cytometer. SYTOX Blue was included in the final cell suspension buffer and was used to exclude dead cells. HEKepo cells directly stained with anti-mouse IgG-Alexa Fluor 647 were used as a negative control. FlowJo software was used for gating and data analysis.

Cell proliferation and viability assay. HEKepo cells grown in well plates (<30% confluency) or inside devices were incubated with 10 µm EdU-Click-iT reagent at 37 °C for 2 h. The membranes of the devices were ripped using a sharp scalpel and the cells were harvested using a trypsin treatment (5 min). The cells were then washed with media to remove excess reagents and separated into two tubes. One tube was kept on ice and subsequently used to assess the percentage viability using SYTOX Blue staining. The other tube was used to complete the EdU staining protocol (permeabilization and reaction with Alexa Fluor 647 Azide reagent) according to the manufacturer's guidelines. The samples were analysed on a BD Fortessa flow cytometer and the data were analysed using the FlowJo software.

Membrane permeability measurement. To determine the permeability of the PCTE membranes, diffusion studies were conducted using a custom-built amber Valia–Chien cell with 2-ml volumes and a 5-mm orifice (PermeGear). The membrane was degassed in a 50% ethanol solution to remove any air bubbles blocking the pores, washed several times in degassed deionized water and placed in the centre of the diffusion cell. One side of the cell was filled with 2 ml deionized water, while the other was filled with 2 ml of a 500 µS cm^{-1} KCl conductivity standard. A conductivity meter (an eDAQ Conductivity isoPod with a miniature dip-in conductivity electrode) was placed in the water side of the diffusion cell and recorded the conductivity of the solution every second for 10 min. To ensure diffusive-dominated transport, both sides of the diffusion cell were connected to an external bath of deionized water using 20 cm of 0.5 mm ID tubing. The conductivity values were converted to concentrations using a standard curve and the flux was calculated as the slope of the concentration-versus-time plot. The normalized permeability value K (m^{-1}) was then calculated using the following equation:

$$J = KA_{\mathrm{m}}D\Delta C$$

where J (mol s^{-1}) is the flux of KCl, A_{m} (m^2) is the area of the membrane, D is the diffusivity of KCl (1.85×10^{-9} m^2 s^{-1}) and ΔC (mol m^{-3}) is the concentration difference between the two sides of the diffusion cell.

Surface characterization. *XPS.* All XPS measurements were done on a Thermo Scientific K-Alpha Plus X-ray photoelectron spectrometer operated at a base pressure of $<5 \times 10^{-8}$ Torr during XPS analysis. The beam area was 400 µm and three locations on the surface were analysed for each sample. The data were analysed and quantified using the Advantage Software (Thermo Fisher Scientific) with the automatic elemental analysis feature.

Confocal Raman microscopy. Devices were washed in deionized water and then sonicated in 1% sodium dodecyl sulfate solution to remove proteins and cells from the surface. Finally, the devices were thoroughly rinsed in deionized water and placed on the quartz coverslip. Excess liquid was absorbed with a tissue. A custom-built near-infrared confocal Raman microscopy system was previously reported[57] and was used in our experiments. Details of the experimental procedure were followed as described elsewhere[24]. Scans were taken for a total 20 z-planes with 20-µm gaps. Afterwards, the planes were manually analysed to identify the device interface, and the spectra were plotted using Prism 7 (GraphPad).

Statistical analysis. Details of the sample size and appropriate statistical test are included in the figure captions. All experiments were repeated at least twice unless specified. The data are expressed as means ± s.e.m. The data were analysed for statistical significance either by unpaired, two-tailed *t*-test or one-way analysis of variance (ANOVA) with Bonferroni multiple comparison correction, as implemented in GraphPad Prism 7. Survival curves were analysed using two-sided Mantel–Cox test. *P* values are indicated in the figure captions.

Reporting Summary. Further information on research design is available in the Nature Research Reporting Summary linked to this article.

Data availability

The main data supporting the findings in this study are available within the paper and its Supplementary Information. The raw and analysed datasets are too numerous to be readily shared publicly. Source data for the figures are available for research purposes from the corresponding author on reasonable request.

Received: 19 June 2019; Accepted: 18 February 2020;
Published online: 30 March 2020

References

1. Towards advanced cell therapies. *Nat. Biomed. Eng.* **2**, 339–340 (2018).
2. Sedlmayer, F., Aubel, D. & Fussenegger, M. Synthetic gene circuits for the detection, elimination and prevention of disease. *Nat. Biomed. Eng.* **2**, 399–415 (2018).
3. Aijaz, A. et al. Biomanufacturing for clinically advanced cell therapies. *Nat. Biomed. Eng.* **2**, 362–376 (2018).
4. Xie, M. et al. β-cell-mimetic designer cells provide closed-loop glycemic control. *Science* **354**, 1296–1301 (2016).
5. Kojima, R. et al. Designer exosomes produced by implanted cells intracerebrally deliver therapeutic cargo for Parkinson's disease treatment. *Nat. Commun.* **9**, 5066 (2018).
6. Power, A. T. et al. Carrier cell-based delivery of an oncolytic virus circumvents antiviral immunity. *Mol. Ther.* **15**, 123–130 (2007).
7. Chassin, H. et al. Sensing and responding to allergic response cytokines through a genetically encoded circuit. *Nat. Commun.* **8**, 1101 (2017).
8. Pagliuca, F. W. et al. Generation of functional human pancreatic β cells in vitro. *Cell* **159**, 428–439 (2014).
9. Millman, J. R. et al. Generation of stem cell-derived β-cells from patients with type 1 diabetes. *Nat. Commun.* **7**, 11463 (2016).
10. Desai, T. & Shea, L. D. Advances in islet encapsulation technologies. *Nat. Rev. Drug Discov.* **16**, 338–350 (2017).
11. Wood, K. J., Issa, F. & Hester, J. Understanding stem cell immunogenicity in therapeutic applications. *Trends Immunol.* **37**, 5–16 (2016).
12. Phelps, E. A. et al. Maleimide cross-linked bioactive PEG hydrogel exhibits improved reaction kinetics and cross-linking for cell encapsulation and in situ delivery. *Adv. Mater.* **24**, 64–70 (2012).
13. An, D. et al. Designing a retrievable and scalable cell encapsulation device for potential treatment of type 1 diabetes. *Proc. Natl Acad. Sci. USA* **115**, E263–E272 (2018).
14. An, D. et al. Developing robust, hydrogel-based, nanofiber-enabled encapsulation devices (NEEDs) for cell therapies. *Biomaterials* **37**, 40–48 (2015).
15. Weir, G. C. Islet encapsulation: advances and obstacles. *Diabetologia* **56**, 1458–1461 (2013).
16. Hwa, A. J. & Weir, G. C. Transplantation of macroencapsulated insulin-producing cells. *Curr. Diab. Rep.* **18**, 50 (2018).
17. Colton, C. K. in *Principles of Tissue Engineering* 543–562 (Academic Press, 2014).
18. Nyitray, C. E. et al. Polycaprolactone thin-film micro- and nanoporous cell-encapsulation devices. *ACS Nano* **9**, 5675–5682 (2015).
19. Chang, R. et al. Nanoporous immunoprotective device for stem-cell-derived β-cell replacement therapy. *ACS Nano* **11**, 7747–7757 (2017).
20. Kumagai-Braesch, M. et al. The TheraCyte device protects against islet allograft rejection in immunized hosts. *Cell Transplant.* **22**, 1137–1146 (2013).
21. Pedraza, E., Coronel, M. M., Fraker, C. A., Ricordi, C. & Stabler, C. L. Preventing hypoxia-induced cell death in beta cells and islets via hydrolytically activated, oxygen-generating biomaterials. *Proc. Natl Acad. Sci. USA* **109**, 4245–4250 (2012).
22. Paul, C. D., Mistriotis, P. & Konstantopoulos, K. Cancer cell motility: lessons from migration in confined spaces. *Nat. Rev. Cancer* **17**, 131–140 (2017).
23. Anderson, J. M., Rodriguez, A. & Chang, D. T. Foreign body reaction to biomaterials. *Semin. Immunol.* **20**, 86–100 (2008).
24. Vegas, A. J. et al. Combinatorial hydrogel library enables identification of materials that mitigate the foreign body response in primates. *Nat. Biotechnol.* **34**, 345–352 (2016).
25. Vegas, A. J. et al. Long-term glycemic control using polymer-encapsulated human stem cell-derived β-cells in immune-competent mice. *Nat. Med.* **22**, 306–311 (2016).
26. Bochenek, M. A. et al. Alginate encapsulation as long-term immune protection of allogeneic pancreatic islet cells transplanted into the omental bursa of macaques. *Nat. Biomed. Eng.* **2**, 810–821 (2018).
27. Pullen, L. C. Stem cell-derived pancreatic progenitor cells have now been transplanted into patients: report from IPITA 2018. *Am. J. Transplant.* **18**, 1581–1582 (2018).
28. Mahou, R., Zhang, D. K. Y., Vlahos, A. E. & Sefton, M. V. Injectable and inherently vascularizing semi-interpenetrating polymer network for delivering cells to the subcutaneous space. *Biomaterials* **131**, 27–35 (2017).

29. Weaver, J. D. et al. Design of a vascularized synthetic poly(ethylene glycol) macroencapsulation device for islet transplantation. *Biomaterials* **172**, 54–65 (2018).
30. Ludwig, B. et al. Transplantation of human islets without immunosuppression. *Proc. Natl Acad. Sci. USA* **110**, 19054–19058 (2013).
31. Whyte, W. et al. Sustained release of targeted cardiac therapy with a replenishable implanted epicardial reservoir. *Nat. Biomed. Eng.* **2**, 416–428 (2018).
32. Lee, K. S. & Ram, R. J. Plastic–PDMS bonding for high pressure hydrolytically stable active microfluidics. *Lab Chip* **9**, 1618–1624 (2009).
33. Lovett, M., Lee, K., Edwards, A. & Kaplan, D. L. Vascularization strategies for tissue engineering. *Tissue Eng. Part B Rev.* **15**, 353–370 (2009).
34. Mendelsohn, A. & Desai, T. Inorganic nanoporous membranes for immunoisolated cell-based drug delivery. *Adv. Exp. Med. Biol.* **670**, 104–125 (2010).
35. Scalea, J., Hanecamp, I., Robson, S. C. & Yamada, K. T-cell-mediated immunological barriers to xenotransplantation. *Xenotransplantation* **19**, 23–30 (2012).
36. Leader, B., Baca, Q. J. & Golan, D. E. Protein therapeutics: a summary and pharmacological classification. *Nat. Rev. Drug Discov.* **7**, 21–39 (2008).
37. Lee, D. E., Son, W., Ha, B. J., Oh, M. S. & Yoo, O. J. The prolonged half-lives of new erythropoietin derivatives via peptide addition. *Biochem. Biophys. Res. Commun.* **339**, 380–385 (2006).
38. Régulier, E., Schneider, B. L., Déglon, N., Beuzard, Y. & Aebischer, P. Continuous delivery of human and mouse erythropoietin in mice by genetically engineered polymer encapsulated myoblasts. *Gene Ther.* **5**, 1014–1022 (1998).
39. Schweicher, J., Nyitray, C. & Desai, T. A. Membranes to achieve immunoprotection of transplanted islets. *Front. Biosci.* **19**, 49–76 (2014).
40. Chong, A. S., Alegre, M.-L., Miller, M. L. & Fairchild, R. L. Lessons and limits of mouse models. *Cold Spring Harb. Perspect. Med.* **3**, a015495 (2013).
41. Tucker, S. P., Melsen, L. R. & Compans, R. W. Migration of polarized epithelial cells through permeable membrane substrates of defined pore size. *Eur. J. Cell Biol.* **58**, 280–290 (1992).
42. Bryers, J. D., Giachelli, C. M. & Ratner, B. D. Engineering biomaterials to integrate and heal: the biocompatibility paradigm shifts. *Biotechnol. Bioeng.* **109**, 1898–1911 (2012).
43. Whyte, W. et al. Sustained release of targeted cardiac therapy with a replenishable implanted epicardial reservoir. *Nat. Biomed. Eng.* **2**, 416–428 (2018).
44. Zhang, L. et al. Zwitterionic hydrogels implanted in mice resist the foreign-body reaction. *Nat. Biotechnol.* **31**, 553–556 (2013).
45. Smith, R. S. et al. Vascular catheters with a nonleaching poly-sulfobetaine surface modification reduce thrombus formation and microbial attachment. *Sci. Transl. Med.* **4**, 153ra132 (2012).
46. Xie, X. et al. Reduction of measurement noise in a continuous glucose monitor by coating the sensor with a zwitterionic polymer. *Nat. Biomed. Eng.* **2**, 894–906 (2018).
47. Jin, X., Yuan, J. & Shen, J. Zwitterionic polymer brushes via dopamine-initiated ATRP from PET sheets for improving hemocompatible and antifouling properties. *Colloids Surf. B Biointerfaces* **145**, 275–284 (2016).
48. Veiseh, O. et al. Size- and shape-dependent foreign body immune response to materials implanted in rodents and non-human primates. *Nat. Mater.* **14**, 643–651 (2015).
49. Tireli, M. et al. Solvent-free copper-catalyzed click chemistry for the synthesis of *N*-heterocyclic hybrids based on quinoline and 1,2,3-triazole. *Beilstein J. Org. Chem.* **13**, 2352–2363 (2017).
50. Régulier, E., Schneider, B. L., Déglon, N., Beuzard, Y. & Aebischer, P. Continuous delivery of human and mouse erythropoietin in mice by genetically engineered polymer encapsulated myoblasts. *Gene Ther.* **5**, 1014–1022 (1998).
51. Sommer, B. et al. Long-term doxycycline-regulated secretion of erythropoietin by encapsulated myoblasts. *Mol. Ther.* **6**, 155–161 (2002).
52. Weber, L. M. & Anseth, K. S. Hydrogel encapsulation environments functionalized with extracellular matrix interactions increase islet insulin secretion. *Matrix Biol.* **27**, 667–673 (2008).
53. Suzuki, K. et al. Function and survival of macroencapsulated syngeneic islets transplanted into streptozocin-diabetic mice. *Transplantation* **66**, 21–28 (1998).
54. Neufeld, T. et al. The efficacy of an immunoisolating membrane system for islet xenotransplantation in minipigs. *PLoS ONE* **8**, e70150 (2013).
55. Salehi, S. & Reed, E. F. The divergent roles of macrophages in solid organ transplantation. *Curr. Opin. Organ Transpl.* **20**, 446–453 (2015).
56. Morris, D. L. Minireview: emerging concepts in islet macrophage biology in type 2 diabetes. *Mol. Endocrinol.* **29**, 946–962 (2015).
57. Kang, J. W. et al. Combined confocal Raman and quantitative phase microscopy system for biomedical diagnosis. *Biomed. Opt. Express* **2**, 2484–2492 (2011).

Acknowledgements

This work was supported by a JDRF grant (2-SRA-2019-714-S-B) and Leona M. and Harry B. Helmsley Charitable Trust Foundation Grant (2017PG-T1D027) to D.G.A. and R.L. S.B. was supported by the National Institutes of Health and NIBIB (K99EB025254) and a JDRF Postdoctoral Fellowship (PDF-2015-90-A-N). L.R.V. and A.F. were supported by the NSF Graduate Research Fellowship Program. S.J. was supported by the Mazumdar-Shaw oncology fellowship. O.V. was supported by a DOD/CDMRP postdoctoral fellowship (W81XWH-13-1-0215). D.L.G. is supported by the National Institutes of Health (UC4 DK104218). We acknowledge S. K. Aresta-Dasilva, C. Landry and A. Nguyen for assistance with the animal experiments. We also acknowledge S. Hrvatin for discussions. This work was supported in part by the Koch Institute Support (core) Grant P30-CA14051 from the National Cancer Institute. We thank the Koch Institute Swanson Biotechnology Center for technical support (specifically the Histology, Proteomics and Flow Cytometry core facilities). We also acknowledge the use of resources at the W. M. Keck Biological Imaging Facility and the Genomics core at the Whitehead Institute. This work was performed in part at the Center for Nanoscale Systems, a member of the National Nanotechnology Coordinated Infrastructure network, which is supported by the National Science Foundation under NSF award number 1541959. The Center for Nanoscale Systems is part of Harvard University.

Author contributions

S.B. and D.G.A. conceived the device, designed the study and wrote the manuscript. S.B., L.R.V., D.T., S.J., C.M., A.W., A.F., Y.T. and C.B. conducted the experiments. V.Y. helped to develop the surface modification method. J.H.-L. and G.C.W. isolated the rat islets and provided technical expertise. O.V., D.L.G. and R.L. provided conceptual advice and technical support. D.G.A. and R.L. supervised the study. All authors discussed the results and commented on the manuscript.

Competing interests

D.G.A., R.L. and O.V. are founding scientists of Sigilon Therapeutics—a biotechnology company based in Cambridge, Massachusetts, United States that produces anti-fibrotic materials for cell-based therapies. For a list of entities with which R.L. is involved, compensated or uncompensated, see https://www.dropbox.com/s/yc3xqb5s8s94v7x/Rev%20Langer%20COI.pdf?dl=0.

Additional information

Supplementary information is available for this paper at https://doi.org/10.1038/s41551-020-0538-5.

Correspondence and requests for materials should be addressed to D.G.A.

Reprints and permissions information is available at www.nature.com/reprints.

Publisher's note Springer Nature remains neutral with regard to jurisdictional claims in published maps and institutional affiliations.

nature research

Corresponding author(s): Daniel Anderson

Last updated by author(s): Jan 15, 2020

Reporting Summary

Nature Research wishes to improve the reproducibility of the work that we publish. This form provides structure for consistency and transparency in reporting. For further information on Nature Research policies, see Authors & Referees and the Editorial Policy Checklist.

Statistics

For all statistical analyses, confirm that the following items are present in the figure legend, table legend, main text, or Methods section.

n/a	Confirmed	
☐	☒	The exact sample size (*n*) for each experimental group/condition, given as a discrete number and unit of measurement
☐	☒	A statement on whether measurements were taken from distinct samples or whether the same sample was measured repeatedly
☐	☒	The statistical test(s) used AND whether they are one- or two-sided *Only common tests should be described solely by name; describe more complex techniques in the Methods section.*
☐	☒	A description of all covariates tested
☐	☒	A description of any assumptions or corrections, such as tests of normality and adjustment for multiple comparisons
☐	☒	A full description of the statistical parameters including central tendency (e.g. means) or other basic estimates (e.g. regression coefficient) AND variation (e.g. standard deviation) or associated estimates of uncertainty (e.g. confidence intervals)
☐	☒	For null hypothesis testing, the test statistic (e.g. *F*, *t*, *r*) with confidence intervals, effect sizes, degrees of freedom and *P* value noted *Give P values as exact values whenever suitable.*
☒	☐	For Bayesian analysis, information on the choice of priors and Markov chain Monte Carlo settings
☒	☐	For hierarchical and complex designs, identification of the appropriate level for tests and full reporting of outcomes
☒	☐	Estimates of effect sizes (e.g. Cohen's *d*, Pearson's *r*), indicating how they were calculated

Our web collection on statistics for biologists contains articles on many of the points above.

Software and code

Policy information about availability of computer code

Data collection	FACS data were collected from the LSR Fortessa flow cytometer with BD FACSDiva v8.0.3 software. Confocal images were acquired using the Zeiss ZEN v2.3 software. XPS spectrum data was collected with the Advantage v3.0 software. Absorbance, luminescence and fluorescence on a microplate reader was collected from a Tecan infinite 2000 PRO by using i-Control v1.8.
Data analysis	PRISM v7 was used to plot data and perform all statistical analyses. Flow data was analysed on FlowJo v 10.5. All images were processed by using ImageJ v1.52n. XPS spectrum data were analysed on Advantage v3.0 software. Mass-spectrum files were processed via Proteome Discoverer v2.4.1 while nanostring data were processed via nSolver v4.0.

For manuscripts utilizing custom algorithms or software that are central to the research but not yet described in published literature, software must be made available to editors/reviewers. We strongly encourage code deposition in a community repository (e.g. GitHub). See the Nature Research guidelines for submitting code & software for further information.

Data

Policy information about availability of data

All manuscripts must include a data availability statement. This statement should provide the following information, where applicable:

- Accession codes, unique identifiers, or web links for publicly available datasets
- A list of figures that have associated raw data
- A description of any restrictions on data availability

The main data supporting the findings in this study are available within the paper and its supplementary information. The raw and analysed datasets are too numerous to be readily shared publicly. Source data for the figures are available for research purposes from the corresponding author on reasonable request.

Field-specific reporting

Please select the one below that is the best fit for your research. If you are not sure, read the appropriate sections before making your selection.

☒ Life sciences ☐ Behavioural & social sciences ☐ Ecological, evolutionary & environmental sciences

For a reference copy of the document with all sections, see nature.com/documents/nr-reporting-summary-flat.pdf

Life sciences study design

All studies must disclose on these points even when the disclosure is negative.

Sample size	The sample size was calculated on the basis of predicted between-group differences and the power needed to reach p-values lower than 0.05 (the cutoff for statistical significance in this study).
Data exclusions	No data points were excluded.
Replication	Experiments were in general repeated twice, to confirm the results.
Randomization	Mice cages were randomly allocated to the experimental groups.
Blinding	The experiments were not blinded because all data were quantitatively measured with standard equipment.

Reporting for specific materials, systems and methods

We require information from authors about some types of materials, experimental systems and methods used in many studies. Here, indicate whether each material, system or method listed is relevant to your study. If you are not sure if a list item applies to your research, read the appropriate section before selecting a response.

Materials & experimental systems

n/a	Involved in the study
☐	☒ Antibodies
☐	☒ Eukaryotic cell lines
☒	☐ Palaeontology
☐	☒ Animals and other organisms
☒	☐ Human research participants
☒	☐ Clinical data

Methods

n/a	Involved in the study
☒	☐ ChIP-seq
☐	☒ Flow cytometry
☒	☐ MRI-based neuroimaging

Antibodies

Antibodies used	AF687-conjugated anti-F4/80 (Clone BM8, cat# 123122, Lot# B212680), BV421-conjugated anti- CD3 (clone 17A2, cat# 100228, lot# B237038), and AF647-conjugated anti-mouse IgG (Clone poly 4053, cat# 405322, lot# B223864) were purchased from Biolegend. Cy3-conjugated anti-mouse alpha smooth muscle actin (clone 14A, cat# C6198, lot# 024M4838V) was obtained from Sigma Aldrich. All antibodies were used at 1:100 dilution.
Validation	All antibodies have been validated for target specificity and immunofluorescence applications by the manufacturers for the applications used. Details of the validation can be found on the product page of each antibody. Previous studies citing these products include (doi: 10.1152/ajpendo.00463.2010, 10.1093/femspd/ftv009, 10.1016/j.bpj.2017.05.005, and 10.1038/nmat4290).

Eukaryotic cell lines

Policy information about cell lines

Cell line source(s)	HEK293T cells (CRL-3216) , 3T3 cells (CRL-1658) and C2C12 cells (CRL-1772) were purchased from ATCC.
Authentication	Authentication was provided by the manufacturer. Cells were further authenticated in the laboratory by analysing their morphology and growth rate.
Mycoplasma contamination	Mycoplasma-free cells were purchased. The transformed HEK293T cells used in the animal studies tested negative for contamination by mycoplasma and other pathogens (testing performed by the vendor).
Commonly misidentified lines (See ICLAC register)	

3T3 has been listed as a misidentified cell line. These cells were used as a model fibroblast only for the preliminary in vitro evaluation of the device.

Animals and other organisms

Policy information about studies involving animals; ARRIVE guidelines recommended for reporting animal research

Laboratory animals	Male C57Bl/6J (Stock No: 000664) and BALB/cJ (Stock No: 000651) 6–8 weeks old were obtained from the Jackson Laboratory. Male Sprague-Dawley rats (NTac:SD) 6–8 weeks old were obtained from Taconic.
Wild animals	The study did not involve wild animals.
Field-collected samples	The study did not involve samples collected from the field.
Ethics oversight	All animal procedures were approved by the MIT Committee on Animal Care, and supervised by veterinary staff from the MIT Division of Comparative Medicine.

Note that full information on the approval of the study protocol must also be provided in the manuscript.

Flow Cytometry

Plots

Confirm that:

☒ The axis labels state the marker and fluorochrome used (e.g. CD4-FITC).

☒ The axis scales are clearly visible. Include numbers along axes only for bottom left plot of group (a 'group' is an analysis of identical markers).

☒ All plots are contour plots with outliers or pseudocolor plots.

☒ A numerical value for number of cells or percentage (with statistics) is provided.

Methodology

Sample preparation	FACS was used to detect and quantify the levels of circulating IgG against transplanted HEKepo cells. Healthy and treated animals were bled to collect about 100 µl of serum. 100,000 HEKEpo cells were incubated with 100 µl of 10-fold diluted serum (90 µl PBS and 10 µl of serum) for 2 hrs at 4°C. The cells were washed 2x with cold PBS and incubated with 100 µl of anti- mouse IgG-AF647 (5 µg/mL) for 30 min at 4°C. Finally, the cells were washed and analyzed on the LSR Fortessa Flow cytometer. Sytox blue was included in the final cell suspension buffer and was used to exclude dead cells. Cell proliferation and viability assay: HEKepo cells grown in well plates or inside devices were incubated with 10µM EdU-ClickIT reagent at 37°C for 2 hours. The membranes of the devices were ripped using a sharp scalpel, and the cells harvested using a trypsin treatment (5 min). The cells were then washed with media to remove excess reagents, and separated into two tubes. One tube was kept on ice and subsequently used to asses viability using Sytox blue staining. The other tube was used to complete the EdU staining protocol according to the manufacturer's guideline. The samples were analysed on a BD Fortessa Flow Cytometer.
Instrument	BD LSR Fortessa Flow cytometer
Software	FlowJo v10.5
Cell population abundance	All viable cells (>95%) were included from the analysis.
Gating strategy	Cells were identified on the basis of FSC/SSC values, and then the Sytox blue signal was used to exclude dead cells from that population.

☒ Tick this box to confirm that a figure exemplifying the gating strategy is provided in the Supplementary Information.